frontiers | Frontiers in Earth Science

ORIGINAL RESEARCH
published: 01 June 2022
doi: 10.3389/feart.2022.888993

(U-Th)/He Geochronology Constraints on Lateritic Duricrust Formation on the Guiana Shield

C. Ansart[1], C. Quantin[1], D. Calmels[1], T. Allard[2], J. Y. Roig[3], R. Coueffe[3], B. Heller[1,2], R. Pinna-Jamme[1], J. Nouet[1], S. Reguer[4], D. Vantelon[4] and C. Gautheron[1]*

[1]GEOPS UMR8148, Université Paris-Saclay, CNRS, Orsay, France, [2]IMPMC, UMR7590 CNRS, Sorbonne Université, MNHN, IRD, Paris, France, [3]BRGM, Orléans, France, [4]SOLEIL Synchrotron, Saint-Aubin, France

Thick regoliths developed under tropical climate, namely, laterites, resulting from long-term and pronounced geochemical and mineralogical rearrangement of the parent rock in response to environmental changes. Little information is available on the timing of laterite and bauxite formations, especially on the chronology of the main weathering episodes responsible for lateritic cover formation on the Guiana shield. For this purpose, we focused on both lateritic and bauxitic duricrusts developed over the Paleoproterozoic Greenstone Belt in the Brownsberg, Suriname. The duricrust samples have a relatively simple mineralogy (i.e., goethite, gibbsite, hematite, and kaolinite) but reveal, when observed at a microscopic scale, a complex history of formation with multiple episodes of dissolution/reprecipitation. The (U-Th)/He dating of 179 Fe-oxides subsamples shows that duricrusts sampled at the top of the Brownsberg plateau have ages ranging from <0.8 Ma to ~19 Ma. In contrast, Fe-oxides extracted from detrital duricrust boulders collected downslope indicate formation ages up to 36 Ma. This age discrepancy may indicate that a main episode of physical erosion affected this region between ca. 30 and 20 Ma. Consistently, the bauxite sampled at the mountaintop indicates a younger phase of formation, with Fe-oxides recementing fragments of a preexisting bauxitic material older than ~15 Ma. Geochronological data also reveal a long-lasting weathering history until the present day, with multiple generations of Fe-oxides in the bauxite and the duricrusts resulting from successive cycles of dissolution and reprecipitation of Fe-oxides associated with redox cycles. This long-lasting weathering history led to geochemical remobilization and apparent enrichment in some relatively immobile elements, such as REE, aluminum, and vanadium, especially in the duricrust sampled at the mountaintop. Our geochronological, mineralogical, and geochemical study of Fe- and Al-crusts from the Brownsberg mountain provide constraints on the evolution of environmental conditions prevailing since the early Oligocene in Suriname.

Keywords: weathering geochronology, (U-Th)/He age dating, laterite, duricrust, Guiana shield, Suriname

OPEN ACCESS

Edited by:
Harilaos Tsikos,
University of Patra, Greece

Reviewed by:
Walid Salama,
Mineral Resources–CSIRO, Australia
Adriana Horbe,
University of Brasilia, Brazil

****Correspondence:***
C. Ansart
claire.ansart@universite-paris-saclay.fr

Specialty section:
This article was submitted to Geochemistry, a section of the journal Frontiers in Earth Science

Received: *03 March 2022*
Accepted: *25 April 2022*
Published: *01 June 2022*

Citation:
Ansart C, Quantin C, Calmels D, Allard T, Roig JY, Coueffe R, Heller B, Pinna-Jamme R, Nouet J, Reguer S, Vantelon D and Gautheron C (2022) (U-Th)/He Geochronology Constraints on Lateritic Duricrust Formation on the Guiana Shield. Front. Earth Sci. 10:888993. doi: 10.3389/feart.2022.888993

INTRODUCTION

Lateritic ferruginous duricrusts and bauxites are common features in the tropical to subtropical landscape, typically located on flat planation surfaces (King, 1962; Théveniaut and Freyssinet, 2002). They result from past or present intense chemical weathering in specific environmental conditions, such as a high precipitation rate with a seasonally contrasted climate along with favorable drainage conditions. These specific conditions can lead to Al or Fe accumulation as kaolinite, Fe-(oxyhydr)oxides (e.g., goethite and hematite—for the sake of simplicity, we will use the term "Fe-oxides" to refer to both Fe-oxides and Fe-oxyhydroxides), or Al-(oxyhydr)oxides (e.g., gibbsite and boehmite) in the weathering profile. A favorable climate (i.e., humid tropical climate) and the absence of tectonic activity contribute to preservation of laterite and bauxite from dismantling for long periods of time, making them potential good records of local past environmental conditions (Tardy and Roquin, 1998; Girard et al., 2000; Vasconcelos et al., 2015; Yapp and Shuster, 2017), and they are useful in investigating the response of weathering processes to climatic variations. However, extracting information on past environmental conditions from duricrust can be complex as secondary minerals may undergo multiple cycles of dissolution/reprecipitation through time (Vasconcelos et al., 1994; Balan et al., 2005; Monteiro et al., 2014; Guinoiseau et al., 2021), in response to changing physico-chemical conditions and climate (Tardy and Nahon, 1985; Trolard and Tardy, 1989).

Laterites form from successive internal geochemical, biological, and geomorphological reorganizations that lead to chemical and mineralogical segregation forming different units and facies (Nahon, 1991; Lucas et al., 1993; Tardy, 1993; Levett et al., 2019). Therefore, multiple generations of different ages of the same mineral (e.g., Fe-oxides and kaolinite) can coexist in the same unit of a lateritic profile (Balan et al., 2007; Monteiro et al., 2014; Mathian et al., 2019). Each generation will provide constraints on external chemical conditions, that is, intensity of rainfall and temperature, prevailing during duricrust formation (Bird and Chivas, 1988; Girard et al., 2000; Yapp and Shuster, 2011). Because laterites can be as old as hundreds of millions of years (Retallack, 2010), secondary minerals forming in such weathering systems are good long-term paleoclimatic indicators and can record discrete climatic events (Bird et al., 1992; Girard et al., 2000). For that, Fe-oxides have been widely used to interpret climatic and environmental variations, through their isotopic composition or their crystallization age, as they can be preserved over geological time scales (Girard et al., 2000; Pidgeon et al., 2004; Shuster et al., 2005; Yapp and Shuster, 2011; Vasconcelos et al., 2013; Monteiro et al., 2014; Wells et al., 2019; Yans et al., 2021).

The dynamics of duricrust formation is still debated, especially in remote places, and requires further geochronological investigations of the different minerals forming the duricrust. High-resolution geochronological tools allow us to determine the different coexisting generations of the same mineral and to constrain the formation and evolution of weathering surfaces, for example, $^{40}Ar/^{39}Ar$ on K-bearing minerals (Vasconcelos et al., 1994; Ruffet et al., 1996; Hénocque et al., 1998; Carmo and Vasconcelos, 2006; Beauvais et al., 2008; Riffel et al., 2015; Deng et al., 2016), (U-Th)/He dating on Fe-oxides (Shuster et al., 2005; Heim et al., 2006; Danišík et al., 2013; Monteiro et al., 2014; Riffel et al., 2016; Allard et al., 2018; Wells et al., 2019; Anand et al., 2021; Heller et al., 2022), or electron paramagnetic resonance (EPR) on kaolinite (Balan et al., 2005; Allard et al., 2018). Iron oxide, a mineral ubiquitous in lateritic profiles, has proven its usefulness in the study of weathering episodes at the scale of a regolith (Shuster et al., 2005; Bernal et al., 2006; Monteiro et al., 2014; Riffel et al., 2016; Allard et al., 2018), which explains why the (U-Th)/He dating methods are widely used for laterite material.

The latitudinal stability of the Guiana shield which has been under tropical climate since ~100 Ma (Tardy and Roquin, 1998; Théveniaut and Freyssinet, 1999) favored the development of deep lateritic profiles and their preservation due to low erosion rate (Stallard, 1988; Shuster et al., 2005). However, major geodynamic events during the Tertiary are known to have affected the climate, and thus the dynamic of regolith formation, at the global scale (Zachos et al., 2008; Westerhold et al., 2020) and, more locally, in South America, for example, the Andean uplift (Hoorn et al., 2010; Jeffery et al., 2012). Little is known about the timing of laterite and bauxite formation in this area because only rare paleomagnetic dating and palynological and sedimentary constraints exist (van der Hammen and Wymstra, 1964; Wong, 1986; Wong, 1994; van der Hammen and Hooghiemstra, 2000; Théveniaut and Freyssinet, 2002). Little absolute dating was performed on laterite from northeastern French Guiana (Heller et al., 2022) and the Northern Amazon basin (Allard et al., 2018, 2020; Mathian et al., 2020), while the geochronology of laterites and bauxites from south and central Amazonia and the Brazilian shield is more documented (Vasconcelos et al., 1994; Ruffet et al., 1996; Théveniaut and Freyssinet, 2002; Shuster et al., 2005; Monteiro et al., 2018; Albuquerque et al., 2020).

This study aims at giving new constraints on the timing of laterite formation in the Guiana Shield (Suriname). In order to constrain the profile formation in this region, we studied duricrust samples from the Brownsberg mountain and performed geochronological investigations using (U-Th)/He geochronology on identified subsamples of the main Fe-oxides (hematite and goethite) from ferruginous duricrust or nodule samples.

GEOLOGICAL AND ENVIRONMENTAL SETTINGS

Sampling sites are located in the Brownsberg nature reserve in Suriname, 100 km south of Paramaribo (**Figure 1**). Suriname lies on the northern part of the Guiana shield which also encompasses Venezuela, Guyana, French Guiana, and the north of Brazil and which is one of the two components of the Amazonian craton separated from the Brazilian shield by the intracratonic Amazon basin (**Figure 1A**). A significant part of Suriname sits on the Paleoproterozoic Greenstone belt formation *ca.* 2.2 Ga (Daoust, 2016; Kroonenberg et al., 2016).

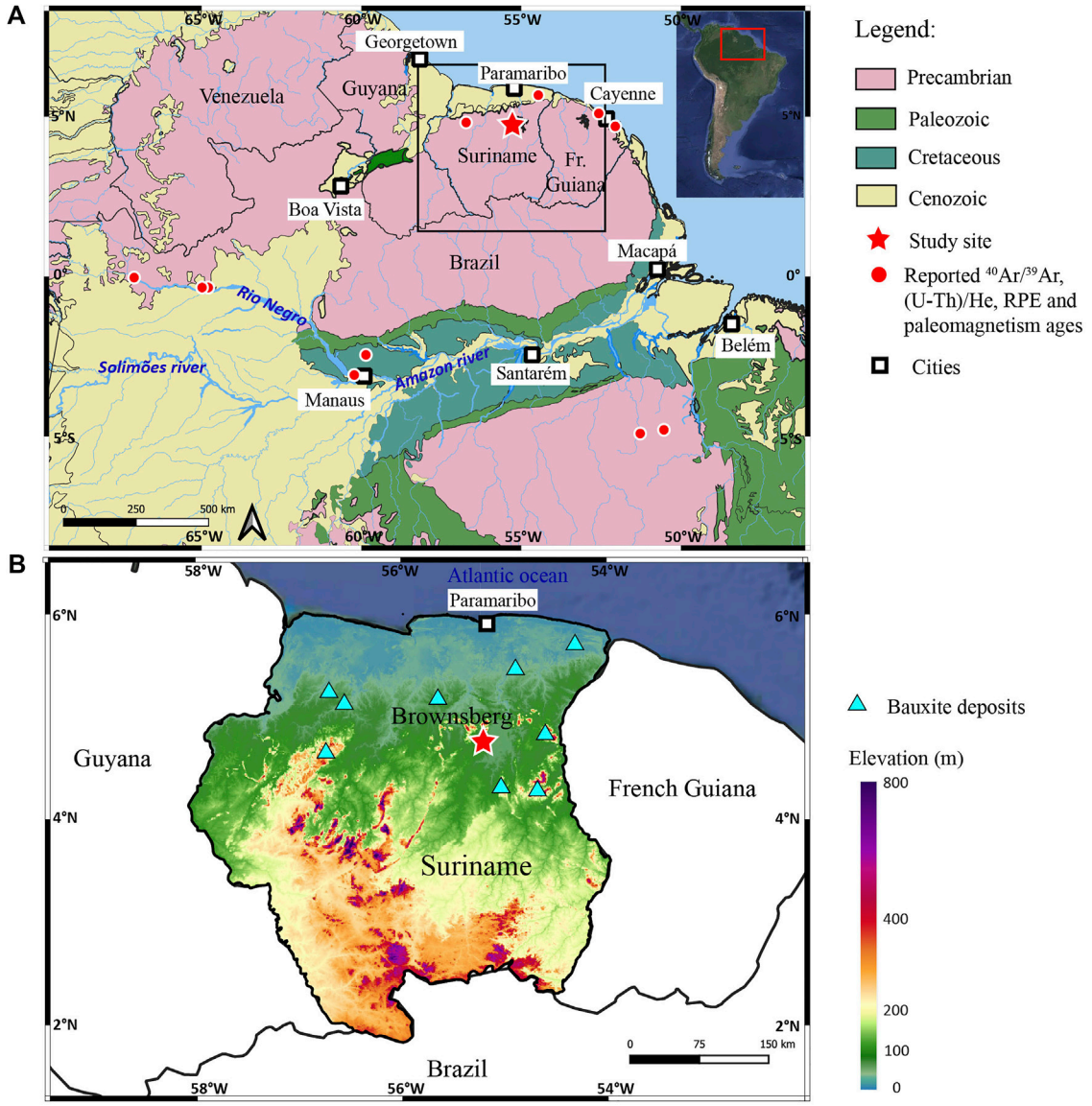

FIGURE 1 | (A) Simplified geological map of the Guiana shield (data from geosgb. cprm.gov.br) with location of dated laterites with 40Ar/39Ar, (U-Th)/He, EPR, or paleomagnetism on the Amazon craton (Vasconcelos et al., 1994; Théveniaut and Freyssinet, 2002; Balan et al., 2005; Allard et al., 2018; Heller et al., 2022) and **(B)** elevation map with known bauxite deposits in Suriname.

The landscape of the Guiana shield is characterized by flat planation surfaces related to uplift/subsidence cycles (King, 1962; Aleva, 1979), on which thick lateritic covers have been formed. Several weathering episodes have been attributed to these formations, according to their elevation and distance from the coast, which are summarized in the studies by Bardossy and Aleva (1990) and Théveniaut and Freyssinet (2002). The Brownsberg mountain is considered to be one of the main bauxitic plateau deposits (Monsels, 2016), which is supposed to have formed during the Paleocene–Eocene (Bardossy and Aleva, 1990; Théveniaut and Freyssinet, 2002), but no absolute dating has been done yet, either in Brownsberg or elsewhere in Suriname. Bauxitic plateau deposits are considered as indicators of a particularly wet and warm climate with a short dry season (Tardy and Roquin, 1998).

The Brownsberg mountain, a ca. 35-km-long and 10-km-wide plateau, belongs to the Paramaka formation, which consists of greenschist metamorphized sedimentary rocks, basalts, and other intermediate to felsic volcanic rocks (Bosma, 1983; Daoust, 2016; Kroonenberg et al., 2016). Precisely, fresh rocks of greenschist metamorphism have been characterized by Eeckhout (1999) on the western flank of the mountain, where falls uncover fresh rock outcrops. The maximum elevation of the Brownsberg mountain is approximately 500 m *a.s.l.* (**Figure 1B**).

The present-day climate of the study area is classified as tropical rainforest climate (Af) in the Köppen climate classification, with a

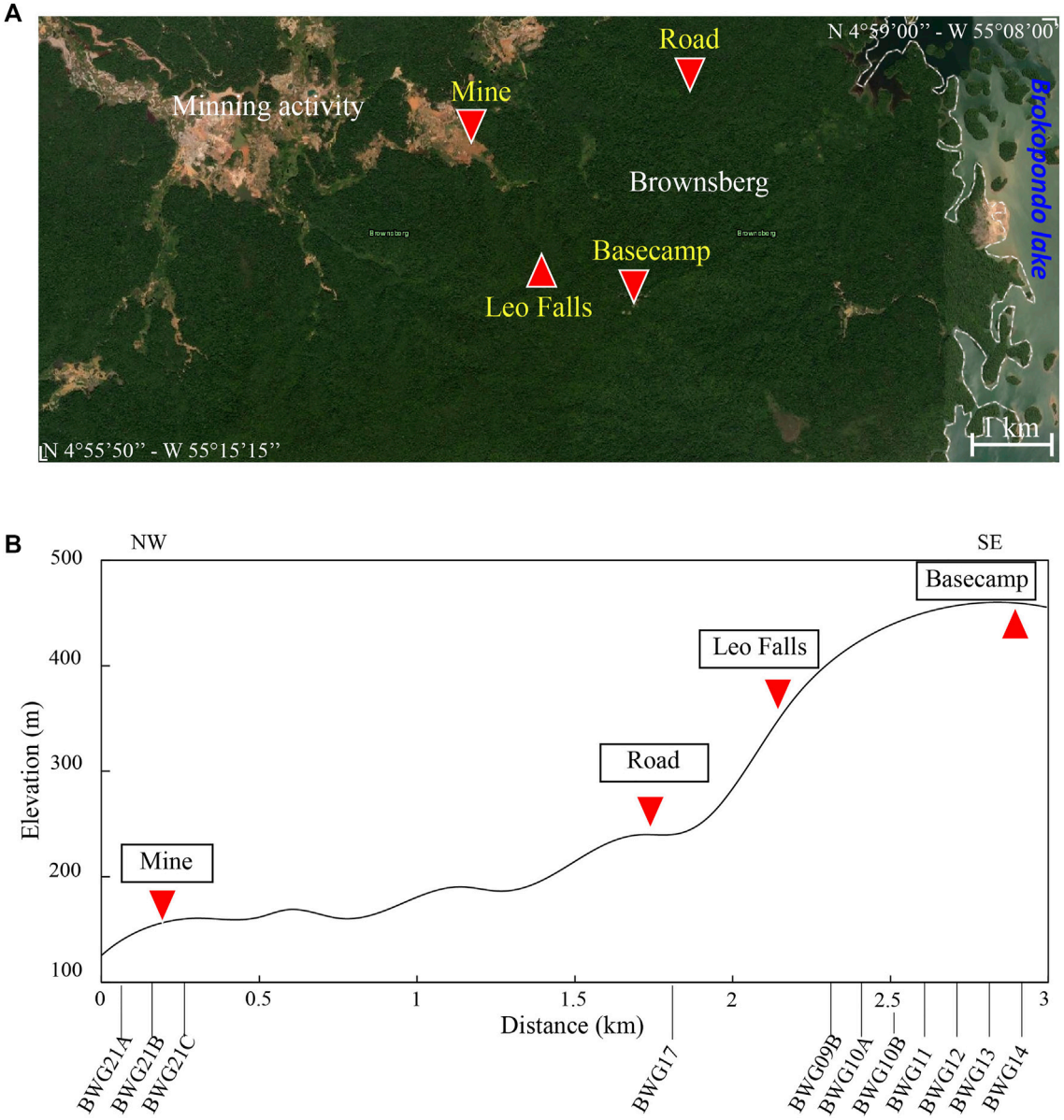

FIGURE 2 | (A) Localization and **(B)** distance between the valley and the mountaintop, with elevation of the sampling site in the Brownsberg area. Note that the position of the Road site is represented here to visualize its elevation, but it is, in fact, located northeast of the Mine–Leo Falls axis.

mean temperature of 25°C, relatively constant through the year (Amatali, 1993). The mean annual rainfall is 2,300 mm.y^{-1} (Bovolo et al., 2018) with two relatively dry seasons (February–April and mid-August–November), related to the position of the Inter-Tropical Convergence zone (ITCZ).

MATERIAL AND METHODS

Sampling Strategy and Sample Description

One bauxite and 10 Fe-lateritic duricrusts were sampled in the Brownsberg mountains. Samples have been collected from well-developed lateritic cover at Leo Falls, while isolated duricrust found next to the road or excavated product from mining activities has been collected (**Figure 2**).

A first set of samples was collected at Leo Falls: one isolated boulder from the nodular zone (BWG09B, ~420 m a.s.l.), five duricrust samples (BWG10A, BWG10B, BWG11, BWG12, and BWG13 from 440 to 460 m a.s.l.), and one bauxite sample containing Fe-oxides (BWG14) collected at an elevation of 465 m a.s.l., at the top of the Brownsberg plateau. A second set of samples was collected in a gold mine (average elevation 170 m a.s.l.), where big boulders of duricrust crop out in an open pit ca. 8 m in the land surface. This site will be called the Mine.

TABLE 1 | Location and elevation of sampling of the different crusts and nodules and main macroscopic characteristics.

Sample	Elevation (m)	Lithotype	Facies-color
***Leo Falls* (4°57′.40″N—55°11′25.90″O)**			
BWG14	465	Bauxite	Pisolithic bauxite with goethite coating
BWG13	463	Fe-duricrust	Massive—homogenous
BWG12	455	Fe-duricrust	Nodular/pisolithic—heterogenous
BWG11	445	Fe-duricrust	Nodular/pisolithic—heterogenous
BWG10B	440	Fe-duricrust	Nodular—homogenous
BWG10A	440	Fe-duricrust	Vacuolar —heterogenous
BWG09B	420	Fe-nodule	Plasmic—heterogenous
***Road* (4°58′14.60″N—55°10′34.80″O)**			
BWG17	250	Fe-duricrust	Pisolithic—homogenous
***Mine* (4°57′58.97″N—55°12′1.73″O)**			
BWG21A	170	Fe-duricrust	Massive—homogenous
BWG21B	170	Fe-duricrust	Massive—homogenous
BWG21C	170	Fe-duricrust	Massive—heterogenous

Three different blocks of duricrust with distinct facies were collected in this site (BWG21A, BWG21B, and BWG21C). These duricrusts are supposed to be eroded material from surrounding plateaus and brought in the depression of the Mine (**Supplementary Figure S1B**). A last sample was collected on a forest road at ~250 m a.s.l. where the duricrust is outcropping. This site will be referred to as the Road. The relative position of each site is shown on **Figure 2A**.

The main characteristics of the samples are summarized in **Table 1**.

Sample Analysis and Characterization

All samples were dried at room temperature and cut into 1- to 2-cm-thick slices. Polished sections were prepared for optical observation. Representative subsamples of nodules and duricrusts (~1–1.5 cm) were included in Epoxy resin and polished for *in situ* characterization by scanning electron microscopy (SEM) with energy-dispersive X-ray spectroscopy (EDS), using the backscattered scanning electron mode (BSD) on a Phenom X Pro (Fondis) microscope at 15 keV and 30 s of acquisition time per point (PANOPLY platform, Université Paris Saclay, France).

A slice of each sample was finely ground for mineralogical and geochemical analysis. The bulk mineralogy of duricrust was determined by XRD on non-oriented bulk powder. The data were acquired on a PANalytical X'Pert Pro diffractometer with Ni-filter Cu Kα radiation and carried out at a voltage of 45 kV, a beam current of 40 mA, and a step size of 0.0167° 2θ, with a counting time of 55 s per step for a total counting time of 4 h, and conducted between 3° 2θ and 80°2θ (PANOPLY platform, Université Paris Saclay, France). The extent of substitution of Al for Fe in goethite was calculated using the method of Schulze (1984) based on the relative variability of 110 and 111 position peaks for Al-substitution, using bulk X-ray diffractograms. The estimated uncertainty is ±2.6 mol % Al when using the method of (Schulze, 1984).

The geochemical composition of bulk samples (major and trace elements, including rare Earth elements) was provided by the SARM analytical service of the CRPG (Nancy, France), using the procedure of Carignan et al. (2001). Major element concentrations were determined by ICP-OES (iCap6500 ThermoFisher) after a lithium tetraborate alkali fusion, and trace elements were quantified by quadrupole ICP-MS (iCapQ ThermoFischer). For further information, see https://sarm.cnrs.fr/pages/roches.html.

Based on macroscopic and microscopic (under a binocular microscope) observations of bulk samples, subsamples *a priori* appropriate for (U-Th)/He geochronology (macroscopically and microscopically homogenous in texture and color with a metallic aspect) were micro-drilled. The obtained material of Fe-oxide was further roughly crushed into several fragments of several hundred micrometers which were subsequently cleaned in an ultrasonic bath with milliQ-water to remove residual clays, without exceeding 30 min and often replacing the water to avoid heating and eventual He loss (Vasconcelos et al., 2013). Representative fragments of dated subsamples were analyzed by SEM-EDS, using the same method as that for bulk fragments.

A set of grains from two selected subsamples (BWG10B_B and BWG21B_B) were also investigated by both μXRD and μXAS at SOLEIL synchrotron (Saint Aubin, France) on DiffAbs and LUCIA beamlines, respectively. These analyses were performed on fine slices (100 μm) of selected aliquots embedded in epoxy resin and carefully polished. Two thin slices of 3 aliquots of the same region of interest were prepared to observed homogeneities or heterogeneities within an Fe-oxide grain. Elemental maps (200 × 200 μm^2) were obtained at 7,250 eV using X-ray fluorescence (XRF) with the Flyscan mode developed at SOLEIL (Leclercq et al., 2015), with a step size of 5 μm, allowing us to obtain the distribution of some metallic elements prior to selecting the region of interest for XANES. These maps were extracted using PyMCa software (Solé et al., 2007). Spatially resolved Fe K-edge X-ray absorption Near Edge Structure (XANES) spectra were obtained on the LUCIA beamline (Vantelon et al., 2016). The data were collected at room temperature under vacuum (5×10^{-2} mbar) using a Si (311) double-crystal monochromator (DCM) with a beam size of 3 × 3 μm^2. The monochromator

was calibrated by setting the first inflexion point of an Fe metallic foil XANES spectrum to 7,112 eV. Five reference spectra were also analyzed: magnetite, chromite, illite, hematite, and goethite. Spectra were collected in both transmission (using a Si diode) and fluorescence (using a 60-mm^2 mono-element SDD) modes for references and only in fluorescence mode for aliquots. XANES spectra for aliquots and references were extracted using Athena software (Ravel and Newville, 2005). The spatially resolved X-ray diffraction (μXRD) analysis and μXRF were performed on the same material on the DIFFABS beamline, synchrotron SOLEIL. The data were collected at room temperature in a transmission mode using an XPAD 2D detector (μXRD) and in fluorescence mode using a SDD 4-elements detector (μXRF) in an angular domain of 7–40° 2θ, with a step of 0.02°2θ and an acquisition of 10 s per step. Both μXRD and μXRF mapping were performed at an energy value of 18 keV using a Si (111) DCM monochromator. Data acquisition was performed either on point mode, on the same point as LUCIA, or on transect mode (using variable step size, from 30 to 50 μm), crossing aliquots, with a beam size of 10 × 10 μm^2.

(U-Th)/He Geochronology

The (U-Th)/He method is based on the quantification of ^{4}He produced by α decay of ^{238}U, ^{235}U, ^{232}Th, and ^{147}Sm, trapped within the crystal structure of a mineral, that is, goethite or hematite. Indeed, U, Th, and Sm may substitute Fe atoms in the crystal structure of goethite, and the contents of He, U, Th, and Sm are required to determine the age, considering the decay constants of ^{235}U, ^{238}U, ^{232}Th, and ^{147}Sm and their radioactive daughter products (Farley, 2002; Pidgeon et al., 2004; Gautheron and Zeitler, 2020). As the He production associated to ^{147}Sm is low in general compared to the other radioactive isotopes, the method is called (U-Th)/He.

A total of 179 Fe-oxide aliquots from 11 ferruginous blocks of nodule, duricrust, or bauxite samples from 3 sites have been dated. Between 2 and 20 (for the BWG14 crust) grains of ~100 μg were selected from each macroscopically homogenous subsample under a binocular microscope. Furthermore, around twenty grains of ~2 mg were used to test He extraction in bigger fragments (e.g., BWG12_E, **Supplementary Figure S1**). Aliquots were precisely sized, weighted, and loaded in a pure Nb tube. Helium content was determined at GEOPS (Gautheron et al., 2021; Université Paris Saclay, France). The method from the study by Allard et al. (2018) was applied, with only one heating cycle necessary to degas the smallest grains and up to three cycles for the largest ones (~2 mg). Each capsule was heated using a diode ytterbium laser under vacuum for 30 min. The heating temperature was kept below 1,000°C in order to avoid actinide volatilization, as observed on hematite (Danišík et al., 2013; Vasconcelos et al., 2013; Hofmann et al., 2020). The heating phase was repeated until all ^{4}He was degassed, especially for the biggest grains. The extracted gas was mixed in the purification line with a known amount of ^{3}He spike and purified from most of the H_2O, CO_2, H_2, and Ar gases using one liquid nitrogen-cooled traps of activated charcoal, titanium sponge, and ST707 and ST701 SAES getters. These gases and helium isotopes (^{3}He and ^{4}He) were measured using a Pfeiffer Prisma Quadrupole mass spectrometer to ensure the purity of the analytical gas (Gautheron et al., 2021). Durango apatite standard materials were degassed to correct for mass spectrometer drift. An internal goethite age and U standard were also used to verify the method. After degassing, the Nb capsules containing aliquots were retrieved and dissolved using the method presented in the study by Allard et al. (2018), with a^{235}U, ^{230}Th, and ^{147}Sm spike volume of 50 μl. The U, Th, and Sm were measured using a high-resolution inductively coupled mass spectrometer Element XR at GEOPS (Université Paris Saclay, France). The analytical uncertainty is lower than 2% (1σ) for U, Th, Sm, and He concentration and 5% for the (U-Th)/He age where equilibrium in the U-Th series is assumed. For ages younger than 0.8 Ma, this statement is not valid anymore, but no correction can be applied as we use ^{235}U and ^{230}Th spikes (Farley, 2002) and thus add a 40% uncertainty on the calculated age. As only one aliquot is characterized with an age younger than 0.8 Ma, the age is reported with the <0.8 Ma value. In addition, a correction of the He loss associated with samples of polycrystallinity and Al content has been applied with 5% ± 5% for the Al-rich samples and 15% ± 15% for the Al-poor samples following the proposition of Bassal et al. (2022).

RESULTS

Petrology, Mineralogy, and Geochemistry of Lateritic Duricrust

Optical images of thin sections of two representative nodular duricrusts highlight either the large-scale homogeneity of Fe-oxide nodules observed in the BWG10B duricrust sample (**Figure 3A**) or the large-scale heterogeneity of Fe-oxide nodules observed in the BWG11 duricrust sample (**Figure 3B**). XRD reveals the presence of goethite, gibbsite, and hematite in all samples except in BWG13 and BWG21B, which do not contain hematite (**Figure 4**). Some remnants of quartz are found in BWG10A, BWG17, and BWG21A, whereas kaolinite is found as booklets in the BWG10A and BWG13 in Leo Falls and in BWG21B in the Mine (**Figures 4**, **5E,I**). Boehmite is present in the bauxite sample of Leo Falls (BWG14). Finally, Ti-oxides are found as anatase or rutile or both in all samples, except in BWG21B. Rietveld refinement performed on samples BWG10B and BWG11 reveals that goethite is the main component of the duricrust (70% and 51%, respectively), while hematite and gibbsite are less abundant with only 25 and 33% and 3 and 9%, respectively.

The calculated Al-substitution (**Table 2**) in goethite ranges between 0% (BWG09A, BWG21A, and BWG21C) and 32% (BWG10B) with Al-substitutions generally being >25% in Leo Falls duricrust, except for the massive duricrust (BWG13) and the bauxite (BWG14) in which the Al-substitution in goethite reaches 7 mol% and 0 mol%, respectively. At a microscopic scale, the extent of Al substitution for Fe in goethite is observed by reflected light microscopy with the gray phase being more substituted than the white ones (**Figure 3F**).

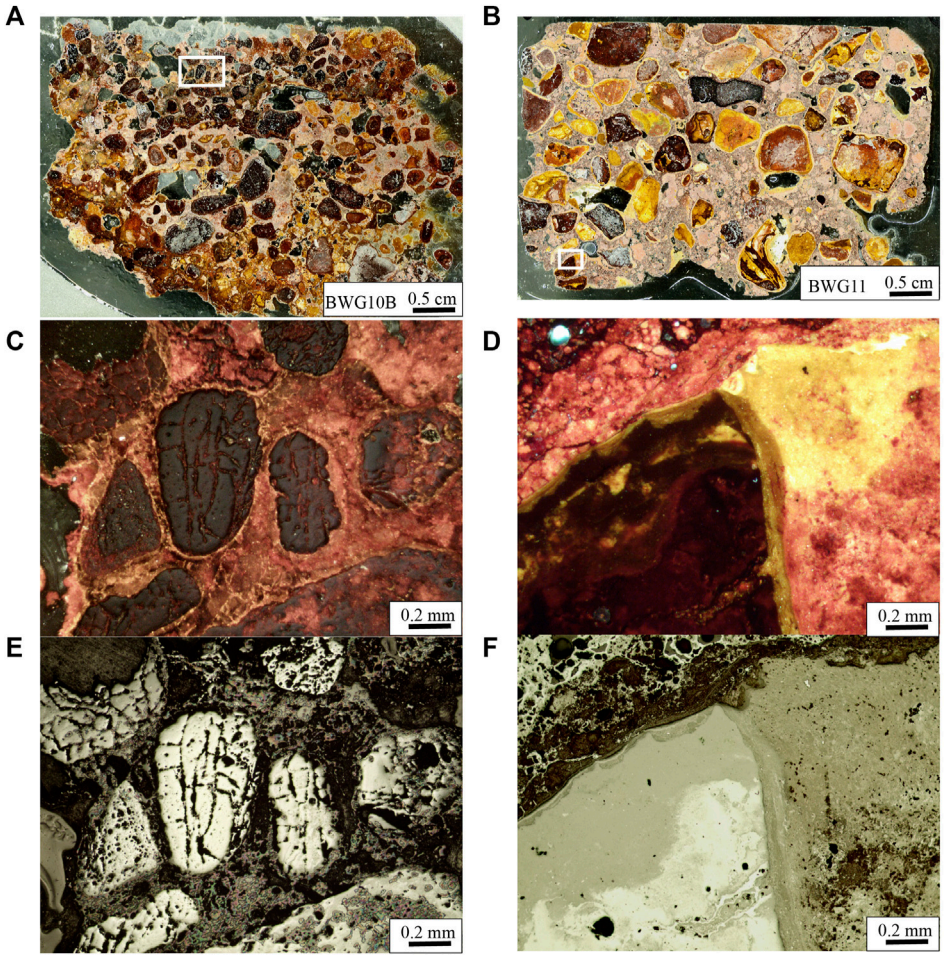

FIGURE 3 | Optical micro-photograph of thin sections of **(A)** BWG10B duricrust and **(B)** BWG11 duricrust, illustrating the Fe-oxide distribution. Magnified view of BWG10B **(C)** shows multiple Fe-oxide grains that look homogenous under reflected light **(E)**, while for BWG11 **(D)**, geochemical heterogeneities can be observed within a single isolated grain **(F)**.

Even though at the macroscopic scale, the selected subsamples seem homogenous and composed of a single Fe-oxide generation (**Figures 3C,E**), optical microscopic and SEM observations reveal that hand-picked samples can vary in texture and composition and pure single generations were rare to detect (**Figures 3**, **5**). Both XANES and μXRD investigations on selected aliquots of generation from two duricrusts (i.e., BWG10B_B from Leo Falls and BWG21B_B from the Mine) show that the selected grains mostly consist of goethite, even though rare hematite has been observed (**Figure 5C**). Colloform Fe-oxides, with varying amounts of Al, Ti, V, and Si, are found (**Figures 5F,G**), indicating different steps of crystallization. For example, the goethitic coatings in the bauxite (BWG14) are at least 3 different generations with distinct Al content (**Figure 5F**). In addition, the μXRD of the BWG10B_B subsample spectra display a 111 goethite peak shift associated with the substitution of Al for Fe in goethite (**Supplementary Figures S5, S6**). This finding is consistent with the substitution observed in the bulk sample (**Table 2**). In the same way, the substitution observed in μXRD of the BWG21B_B sample is similar to the results of the bulk sample, that is, no substitution is observed for goethite.

Kaolinite is preserved in the form of small booklets (ca. 3–4 μm) trapped within the goethite phase found in a few samples, especially in massive duricrust (e.g., BWG13) or massive hand-picked phases (e.g., BWG10A_B, **Figure 5A**). Kaolinite is embedded in goethite, preserving a clayey and porous texture (**Figures 5A,E**).

Scarce inclusions of zircon (**Figure 5D**) and quartz are also observed within Fe-oxides. Yttrium mineral as xenotime (<10 μm) has been reported in the generation BWG10A_A1 (**Figure 5B**). Still, these inclusions are minor compared to the size of the studied Fe-oxide, largely bigger than 100 μm.

Elemental composition is consistent with the mineralogy, with Fe_2O_3 ranging between 34% (BWG14) and 80% (BWG21B) and Al_2O_3 between 3% (BWG21B) and 37% (BWG14), respectively (**Table 2**). The REE content of the duricrust is lower than in the UCC (Taylor and McLennan, 1995), varying from 13 ppm (BWG21C) to 132 ppm (BWG11). The REE content is higher

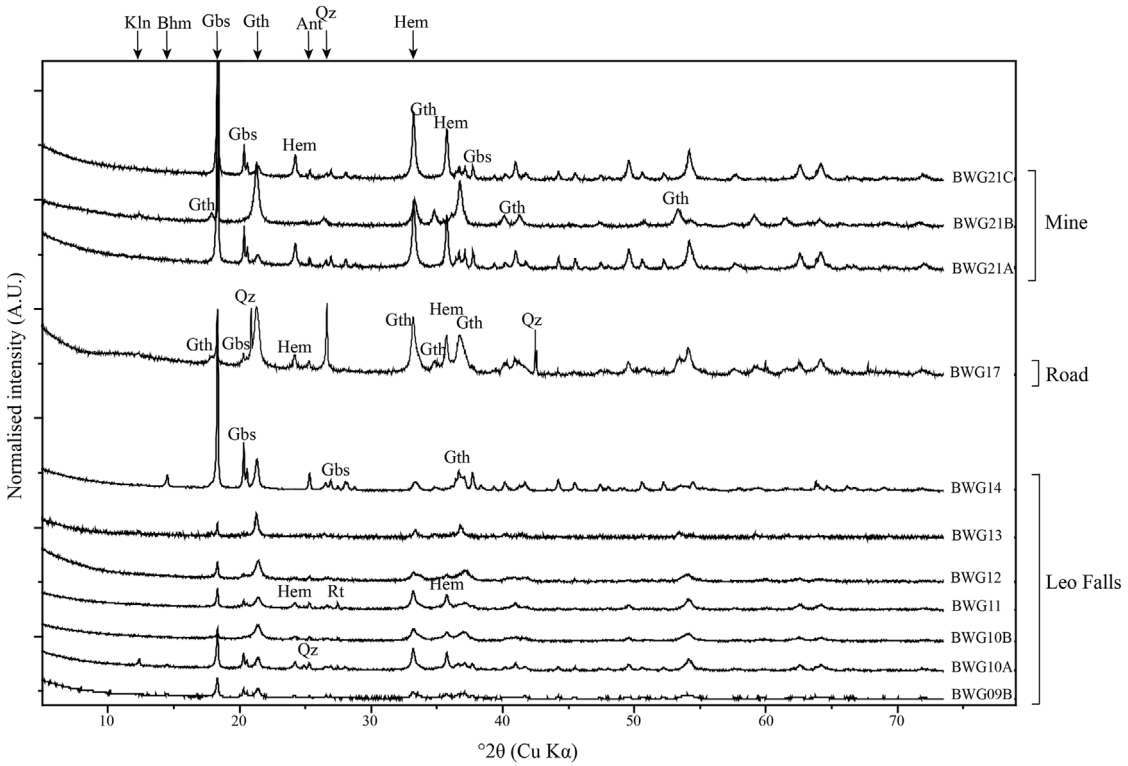

FIGURE 4 | XRD pattern of duricrust samples from each site. With Ant, anatase; Bhm, boehmite; Gbs, gibbsite; Gth, goethite; Hem, hematite; Kln, kaolinite; Qz, quartz; Rt, rutile.

in the Leo Falls duricrust (43–132 ppm) than in the Mine (13–23 ppm) or Road (20 ppm) samples. Concentrations of Th and U are the lowest in the Mine samples with 0.33 ppm (BWG21B) and 0.37 ppm (BWG21A), respectively, and maximum in the BWG11 sample, with 14.8 and 2.8 ppm, respectively.

(U-Th)/He Geochronology on Fe-Oxides

(U-Th)/He ages of Fe-oxides range from 34.4 ± 3.1 Ma to <0.8 Ma, and the age distribution reveals peaks at ~4 Ma, 10–15 Ma, and ~30 Ma (**Figure 6**; **Supplementary Figure S3**).

The ages of Fe-oxides extracted from Leo Falls duricrusts range from early Miocene to Pleistocene (19.5 ± 2.5 Ma and <0.8 Ma), both measured in the sample (BWG13). Mine samples display older ages, between 4.1 ± 0.6 Ma (BWG21A) and 36.0 ± 5.4 Ma (BWG21C). For the Road duricrust, He ages lie between 1.8 ± 0.3 Ma and 24.5 ± 3.7 Ma. Uranium, Th, and Sm contents are highly variable, ranging from 0.03 to 4.6 ppm, 0.01 to 30.3 ppm, and 0 to 2.8 ppm, respectively.

Most dated subsamples show relatively homogenous ages, though exceeding the analytical uncertainty, but intra-subsample variability is observed for ages and U, Th, or Sm content that cannot be explained by uncertainties of measurement (i.e., BWG10B_B, BWG13_A1, BWG13_A2, BWG14_A, BWG17_B, BWG17_C, BWG17_D, BWG21A_B, BWG21B_A, BWG21B_B, BWG21C_A, and BWG21C_B). The standard deviation on age between aliquots from the same subsample can exceed 6 Ma (i.e., BWG21C_A) but can also be lower than 1 Ma (i.e., BWG09B_A, BWG09B_B, BWG10A_A2, BWG10B_A1, and BWG13_B). Age variability is greater when the average age is older.

DISCUSSION

(U-Th)/He Age Significance

The three studied sites yield Fe-oxide He-ages from the late Eocene (36.0 ± 5.4 Ma) to the Pleistocene (<0.8 Ma) (**Figure 6**). A large variability was noticed between extracted subsamples even from the same duricrust slice but also, in some cases, between replicates of the same subsample. Indeed, dispersed ages are generally associated with distinct U, Th, or Sm content (**Figure 6**). In fact, many factors are likely to influence the He content in Fe-oxides, for example, helium loss (Hofmann et al., 2017), mineral inclusions richer in He, U, or Th than Fe-oxides (Cornu et al., 2009; Vasconcelos et al., 2013; Monteiro et al., 2014; Riffel et al., 2016), Fe-oxide grain size and crystallite size (Shuster et al., 2005), or mixture of Fe-oxides of different ages (Heller et al., 2022). To avoid U, Th, or Sm loss, the heating phase was carefully undertaken to degas all He content, and temperature was regularly monitored. In addition, internal goethite standards were analyzed to check that no U, Th, or Sm was lost during the heating process.

U–Th-rich mineral inclusions (e.g., apatite, zircon, titanite, xenotime, and monazite) might be responsible for

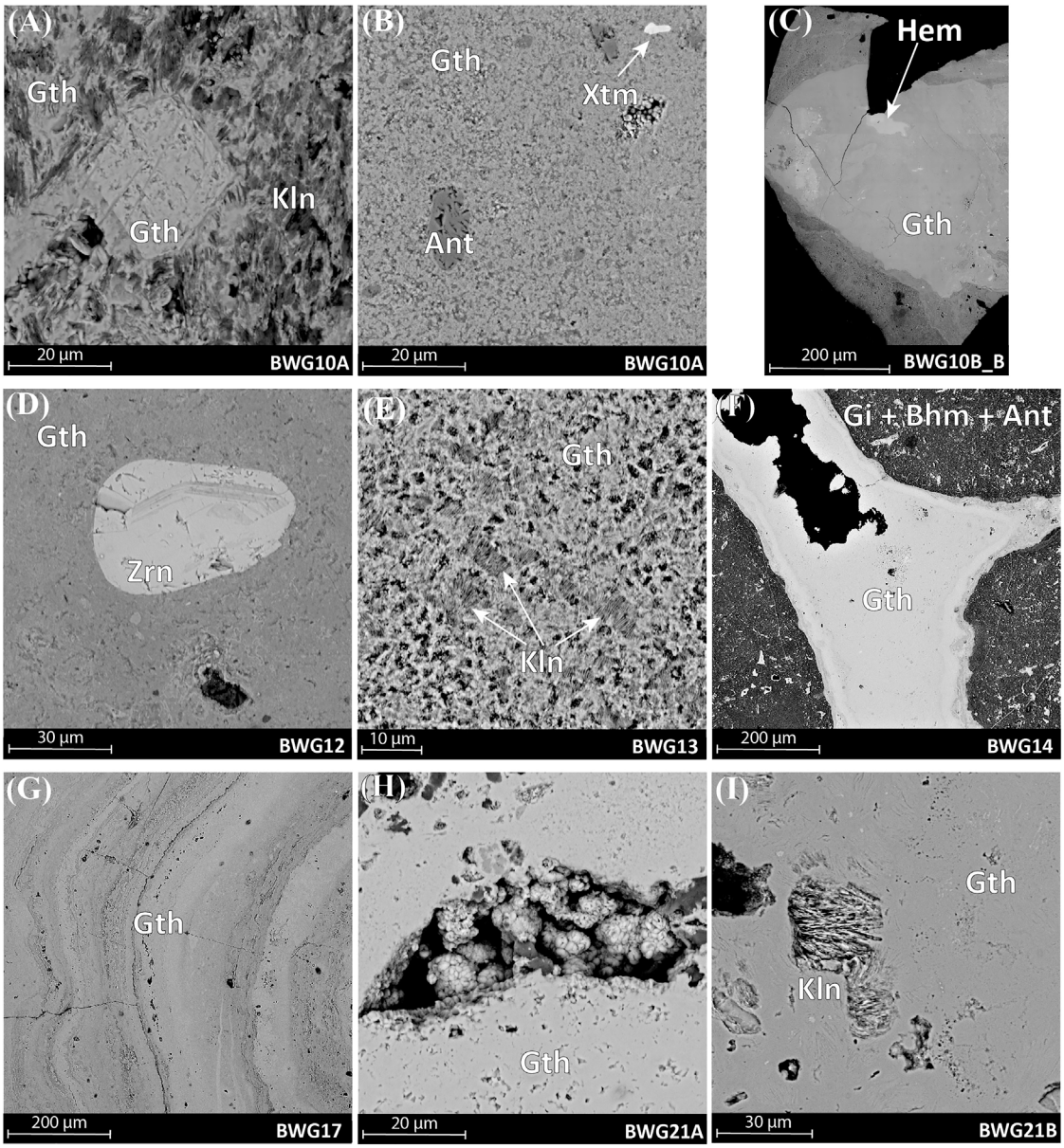

FIGURE 5 | Scanning electron microscopy images. **(A)** Detrital goethite (Gth) surrounded by intergrown kaolinite (Kln) booklets and checkered secondary goethite. **(B,D)** Contaminant can be present in dated aliquots, for example, anatase (Ant), xenotime (Xtm), or zircon (Zrn). **(C)** Goethite is the main Fe-oxide found in the Brownsberg sample, but hematite (Hem) can be observed. **(E,I)** The massive duricrust from Leo Falls (BWG13) and the Mine (BWG21B) displays epigenetic replacement of kaolinite booklets by goethite. **(F,G)** Colloform goethite displaying various Al, Si, or Ti contents traduce long-term weathering under different environmental conditions. **(F)** The bauxite is mainly composed of gibbsite (Gbs) eventually accompanied by boehmite (Bhm) and anatase (Ant). **(H)** Polycrystalline texture of pure goethite in BWG21A.

heterogenous age within a single generation, because their He content is higher than that of Fe-oxides, leading to the measurement of older ages (Vermeesch et al., 2007). Although the dated grains seem of relatively high-purity Fe-oxide (i.e., uniform dark color and metallic luster), microscopic observations show mineral inclusions. SEM observations reveal that few xenotime and zircon minerals can be expected in some samples and subsamples (**Figures 5B,D**). Xenotime is often associated with old metamorphic rocks of low grade metamorphism, that is, greenschist (Spear and Pyle, 2002), which is compatible with the local geology (Eeckhout, 1999; Kroonenberg et al., 2016). Farley and Stockli (2002) showed that xenotime contains high Th and U concentrations but with higher temperature for complete He degassing than Fe-oxides (~1,300°C for xenotime but ~950°C for Fe-oxides). Thus, an excess of U and Th compared to He appears in subsamples containing xenotime inclusions, lowering the age of the dated grain. However, no

TABLE 2 | Chemical concentration of the bulk samples from the 3 sites and calculated Al-substitution from XRD diagram according to Schulze (1984). <L.D. = under detection limit. *For calculated %Al-substitution, results that are negative are set to zero.

	BWG09B	BWG10A	BWG10B	BWG11	BWG12	BWG13	BWG14	BWG17	BWG21A	BWG21B	BWG21C
				Leo Falls				*Road*		*Mine*	
g.kg^{-1}											
SiO_2	9.10	27.70	15.10	24.70	15.36	74.50	11.70	74.90	4.60	22.20	4.10
Fe_2O_3	570	510	666	577	572	639	336	672	596	802	627
TiO_2	13.70	26.40	24.40	36.00	26.16	12.86	34.40	12.93	13.02	0.62	15.11
Al_2O_3	218	251	131	186	212	152	374	104	241	33.07	215
CaO	0.37	0.35	0.42	0.40	0.04	0.06	1.95	< L.D.	0.51	0.38	< L.D.
Na_2O	2.05	1.45	1.45	1.72	0.08	0.08	1.47	< L.D.	< L.D.	< L.D.	< L.D.
K_2O	< L.D.	< L.D.	< L.D.	0.31	< L.D.	< L.D.	< L.D.	< L.D.	< L.D.	< L.D.	< L.D.
MgO	1.23	1.85	< L.D.	0.18	0.04	0.09	3.91	< L.D.	< L.D.	< L.D.	< L.D.
MnO	0.24	0.25	0.26	0.29	0.12	0.18	0.29	0.30	0.17	0.28	< L.D.
LOI	186	181	161	173	175	121	237	135	148	132	140
ppm											
Th	13.72	12.97	11.76	14.78	12.83	7.04	11.73	4.64	2.93	0.33	5.57
U	2.07	1.69	1.61	2.81	1.35	1.40	1.36	0.78	0.37	0.54	0.51
Th/U	6.63	7.67	7.31	5.25	9.52	5.02	8.63	5.94	7.84	0.62	10.84
V	3,221	1,648	3,760	1,497	3,393	1888	441	1,021	260	79.9	760
Y	8.04	16.33	15.53	28.53	6.48	11.73	10.60	3.76	3.30	9.00	3.20
ppm											
La	9.52	17.4	18.0	30.2	13.8	8.3	14.0	4.50	4.04	2.03	2.67
Ce	16.9	28.0	30.3	50.3	23.8	15.6	23.1	7.96	5.80	6.33	4.68
Pr	2.02	3.59	3.70	6.24	3.00	2.15	2.42	0.91	0.76	0.94	0.54
Nd	7.20	13.1	12.9	22.4	11.1	9.1	7.71	3.18	2.46	4.46	1.92
Sm	1.31	2.46	2.31	4.01	1.90	2.37	1.25	0.65	0.47	1.51	0.44
Eu	0.32	0.62	0.59	0.98	0.44	0.76	0.31	0.16	0.12	0.53	0.13
Gd	1.08	2.10	2.01	3.54	1.61	2.76	1.12	0.52	0.38	1.53	0.40
Tb	0.19	0.37	0.37	0.66	0.23	0.49	0.21	0.10	0.07	0.30	0.08
Dy	1.32	2.59	2.62	4.69	1.47	3.49	1.58	0.65	0.51	2.01	0.56
Ho	0.32	0.63	0.61	1.08	0.34	0.66	0.392	0.161	0.125	0.430	0.14
Er	0.98	1.96	1.85	3.25	1.20	2.06	1.31	0.52	0.46	1.19	0.46
Tm	0.16	0.34	0.31	0.52	0.19	0.34	0.23	0.09	0.09	0.17	0.09
Yb	1.25	2.74	2.34	3.76	1.66	2.34	2.02	0.88	0.80	1.15	0.77
Lu	0.23	0.50	0.41	0.64	0.29	0.37	0.39	0.17	0.15	0.16	0.15
ΣREE	42.79	76.43	78.36	132	60.99	50.69	56.06	20.46	16.23	22.74	13.03
%Al-subst	25	26	32	28	27	7	0*	2	0*	3	0*

such excess was observed (**Supplementary Figure S3**) and the yttrium concentrations did not show any enrichment in our subsamples, compared to the upper continental crust (**Table2**; Rudnick and Gao, 2003). Consequently, we hypothesize that remnant xenotime does not impact the present (U-Th)/He data. In all cases, data with abnormally high Th, U, or Sm compared to the He content but also compared to other grains of the same subsample were not considered (**Supplementary Figure S3** , **Supplementary Table S4**) Inversely, grains with too high He content compared to the U–Th–Sm were also removed for further discussion. In total, these grains represent 14 data over 193.

Additionally, the variability in U, Th, and age found in aliquots from the same subsample can result from different generations of Fe-oxides, or simply different Fe-oxides, that developed tightly and are highlighted in SEM observations by a difference in contrast and texture (**Figures 3F**, **5A,C,F,G,I**) (Monteiro et al., 2014; Heller et al., 2022).

Finally, Shuster et al. (2005) pointed out the potential size effect of the dated object (i.e., subsample) on the disparity of measured ages, considering that too large Fe-oxides are formed by multiple generations and not smaller ones. However, in our study, we have observed that the small-sized (~500 μm) dated grains from the BWG12 duricrust (**Supplementary Table S4**) display similar age to larger-sized grains, that is, more than 1 mm (e.g., BWG12_A and BWG12_E10 or BWG12_D and BWG12_G07). In addition, synchrotron analysis also revealed that even at a smaller scale, the selected Fe-oxide grains display heterogeneities (in texture, composition, and presence of different generations). This means that the small-sized grains can also reflect the complex history of the formation of a whole subsample. Nonetheless, the biggest aliquots are prone to containing phase mixtures (e.g., kaolinite) and, consequently, display He deficiency compared to the U–Th–Sm content (**Supplementary Figure S3**) (Wells et al., 2019). All of these considerations have a potential effect on

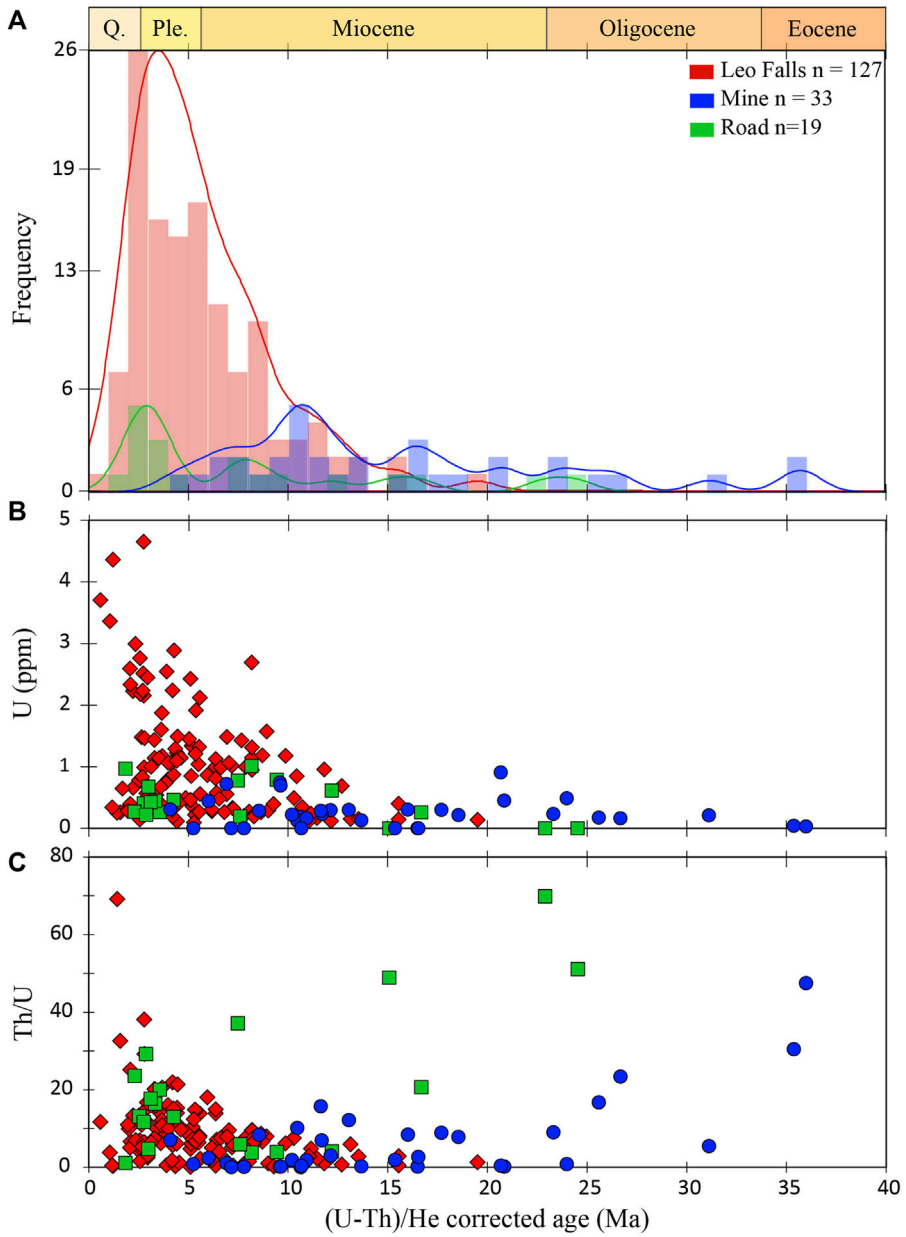

FIGURE 6 | (A) Fe-oxide age repartition in each sampling site. Young Fe-oxides (~3–5 Ma) are the most common, especially at Leo Falls and in the Road duricrust, and Fe-oxides older than Miocene are found in the Mine, with Q, Quaternary; Ple, Pleistocene; Eo, Eocene. **(B)** Evolution of the U concentration and **(C)** Th/U ratios of subsamples according to their (U-Th)/He ages.

measured Fe-oxide age (Shuster et al., 2005; Monteiro et al., 2014; Riffel et al., 2016) and confirm that small aliquots are more appropriate for dating than material in the size range of a millimeter. However, we consider that most of the measured U, Th, and He content is robust and reflect Fe-oxide U and Th content with no addition or loss of He (**Supplementary Figure S3**).

Even though supergene goethite can retain He over geological time scales, 2–20% of natural He can be lost by diffusion for goethite (Shuster et al., 2005). The He diffusion leads to underestimated (U-Th)/He ages due to the polycrystalline nature of supergene Fe-oxides (**Figure 5H**) (Shuster et al., 2005). Bassal et al. (2022) proposed that He retention is linked to the damage dose and the Al-substitution of the Fe-oxide. In addition, porosity and crystallinity of the different generations can impact He retention and lead to younger ages (Farley, 2018). For instance, the porosity increases when goethite is replacing primary minerals such

as kaolinite and are consequently tightly intergrown (e.g., **Figures 5A,E,I**). But the relatively high homogenous amount of He suggests that our samples were not subject to major He loss due to porosity. Synchrotron XRD analysis on Fe-oxide grains (**Supplementary Figure S5, S6**) and calculated %Al substitution in goethite from XRD bulk samples (**Table 2**) highlight significant Al substitutions in goethite from Leo Falls duricrusts (ca. 30% of Al-substitution in the nodular and vacuolar Fe-crusts), that should decrease goethite crystallinity and consequently may increase He retention, due to smaller crystallite size (Fitzpatrick and Schwertmann, 1982; Schulze, 1984; Schwertmann and Carlson, 1994; Vasconcelos et al., 2013). Therefore, we systematically applied the correction for He diffusion to our samples following the consideration of Bassal et al. (2022) (**Supplementary Table S4**).

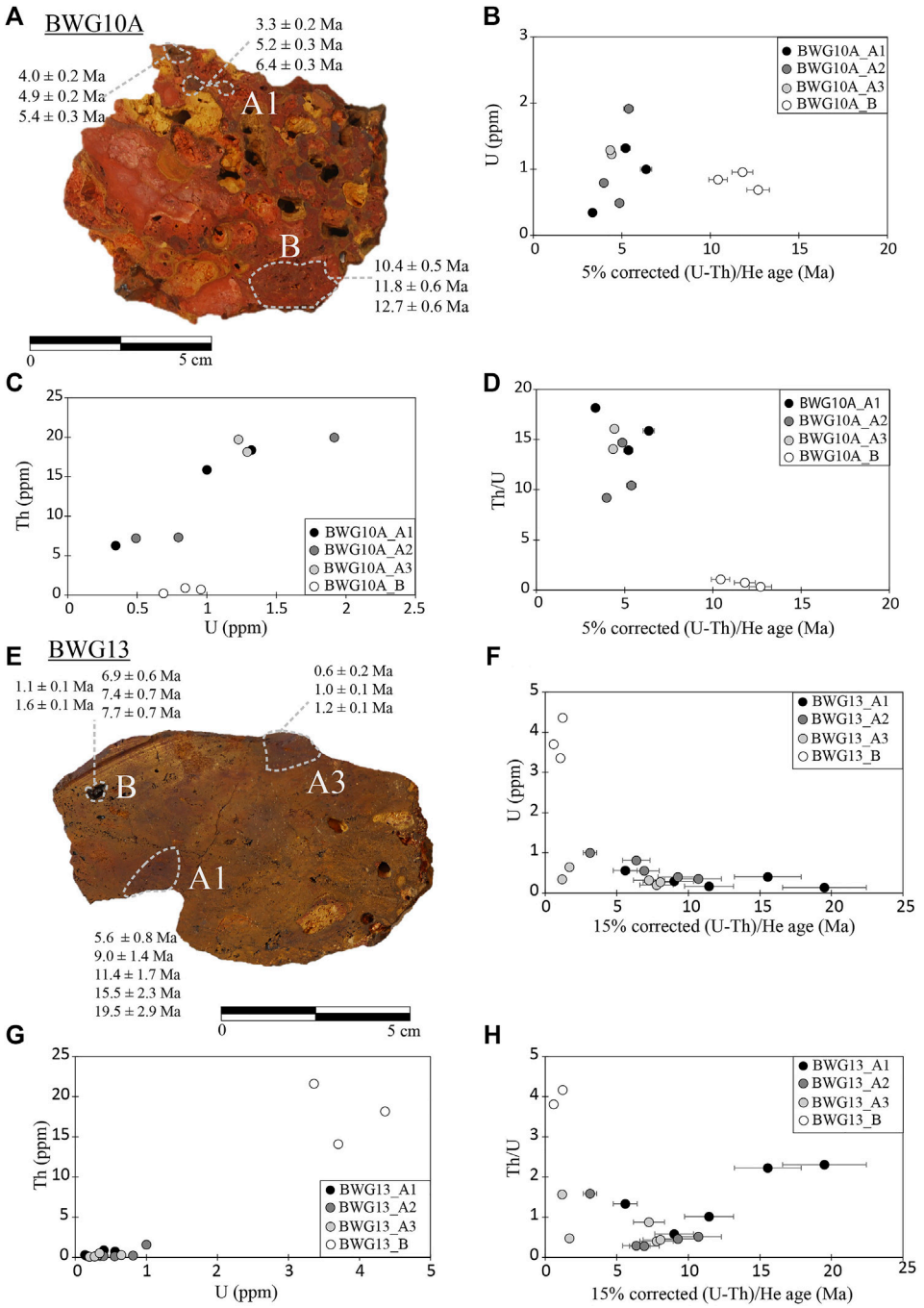

FIGURE 7 | (Continued).

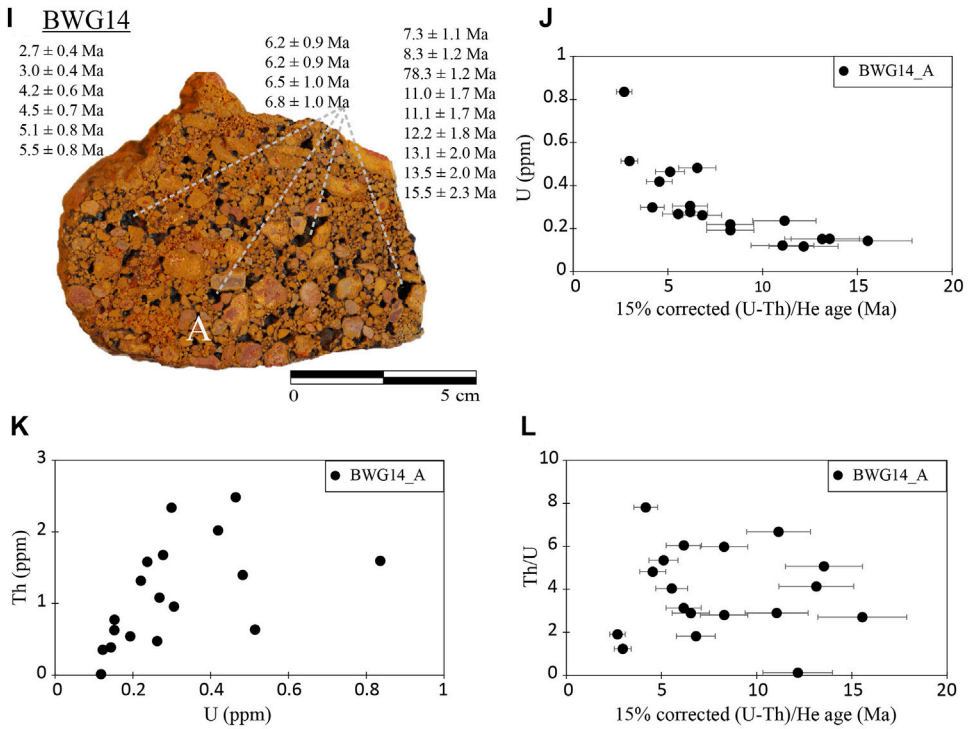

FIGURE 7 | (Continued). **(A)** Picture of the BWG10A, **(E)** BWG13, and **(I)** BWG14 duricrust samples with localization of handpicked subsamples and associated ages. **(B,F,J)** Evolution of U content or **(D,H,L)** Th/U ratio according to the age and **(C,G,K)** binary diagram of Th vs. U for the duricrust samples mentioned above, respectively.

The different grains of each subsample usually display homogenous U and Th concentrations within the same range of values and with similar Th/U ratios (**Figure 7**), attesting to similar weathering history. Even though some selected subsamples display variable Th and U concentrations or distinct ages, the U *vs.* age diagram shows that the generations are usually distributed between two endmembers, with an old U-poor generation and a young U-rich generation (**Figures 6B**, **7B,F**). This trend suggests a progressive evolution of the system or the mixing of these two phases. Indeed, even though U is highly mobile under an oxidizing environment, U can be easily removed from fluids by Fe-oxides either by adsorption or Fe-substitution (Duff et al., 2002; Missana et al., 2003; Kerisit et al., 2011). Thus, the variability in U, Th, and age reflects a mixture of the young U-rich generation and the old U-poor generation and of different origins. The distinct Th vs. U (**Figure 7C**) can traduce a different weathering history of different subsamples with either Fe-precipitation from enriched fluids (BWG10A_B) or replacing silicate minerals, inheriting its Th content (BWG10A_A) (Riffel et al., 2016).

Thus, we can conclude that measured (U-Th)/He ages can inform on the long-term weathering history of the Brownsberg area, with several weathering episodes recorded and preserved through the multiple Fe-oxide generations.

Lateritization and Bauxitization Events in Suriname

The Guiana shield has been exposed to long-term lateritization and bauxitization processes, shaping the landscape with thick lateritic covers sometimes containing Fe- and Al-crusts that evolved through time (Beauvais and Colin, 1993).

The variability of facies and mineralogy at different scales of the studied area reveals the complex history of lateritic and bauxitic duricrusts that experienced several episodes of precipitation of Fe-Al oxides over the Cenozoic. The distribution of the measured ages indicates significant weathering events affecting previously formed secondary minerals, leading to a rejuvenation of the duricrust, due to the possible dissolution of the oldest Fe-oxides and crystallization of new Fe-oxides (**Figure 8**). The oldest age measured in the present study indicates that ferruginization processes were initiated, at least, ca. 35 Myr ago in this part of Suriname. The predominance of goethite in all the samples testifies to high water activity associated with a humid tropical context with only low seasonal contrast (Tardy and Nahon, 1985) that probably persists and intensifies in the early Miocene with bauxite formation (older than 15 Ma). Low-temperature thermochronological investigations (Derycke et al., 2021) and sedimentary data (Wong, 1986; Wong, 1994) reveal that the northern part of the Guiana Shield basement has been exposed to (near-)surface conditions since the late Cretaceous (c.a. 90 Ma), while our study indicates a maximum age of 36.0 ± 5.4 Ma for secondary Fe-oxide formation. The equatorial position of the Guiana Shield and the supposed globally warm and permanently humid climate prevailing during the 90–35 Ma interval would have favored strong weathering processes

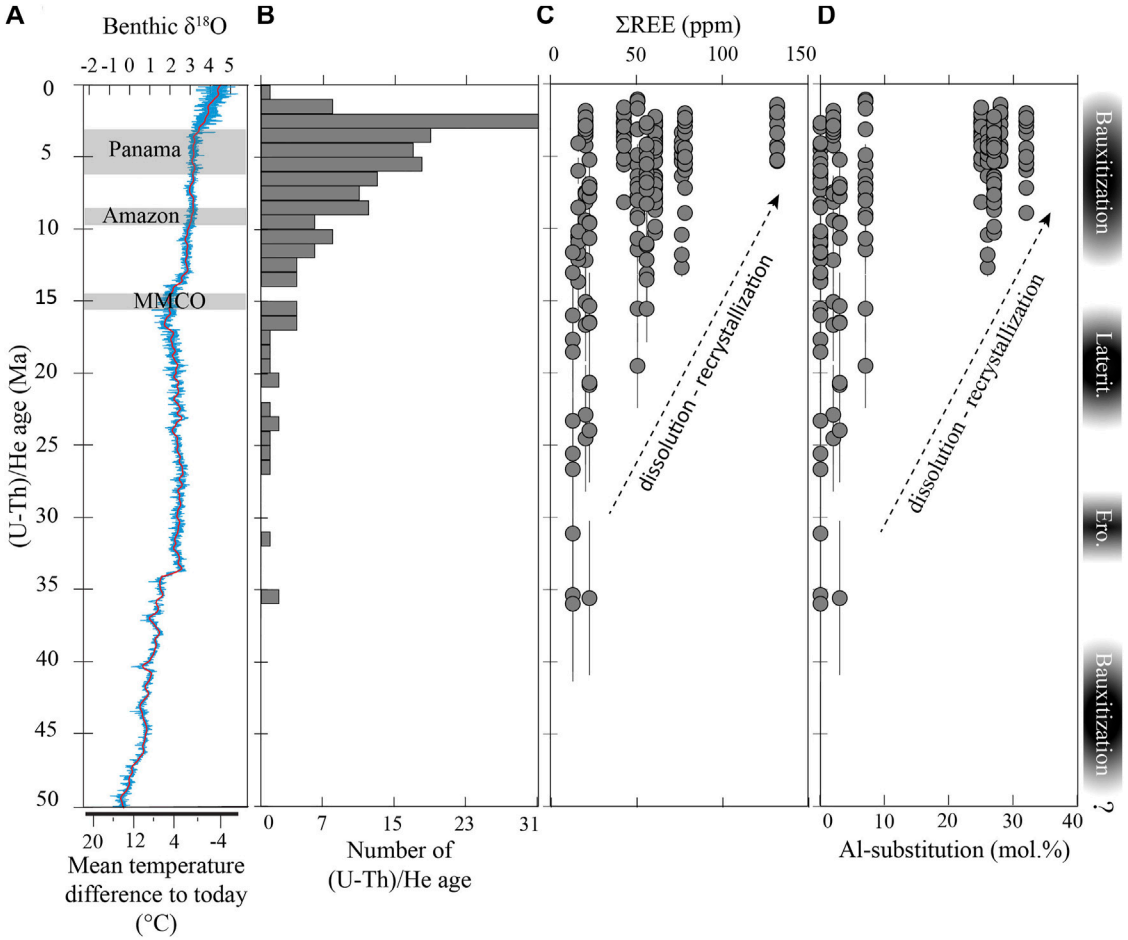

FIGURE 8 | (A) Global evolution of the $\delta^{18}O$ composition of benthic foraminifera from ocean drill cores and global temperature evolution in comparison to actual mean temperature (Westerhold et al., 2020), with major climatic and/or geological events: the mid-Miocene Climate Optimum ca. 15 Ma, the onset of the actual Amazon drainage system ca. 9 Ma, and the closure of the Panama isthmus ca. 7–3 Ma. **(B)** (U-Th)/He age distribution of our dataset. **(C)** Distribution of bulk REE concentrations of duricrust samples in comparison to (U-Th)/He age of subsamples. **(D)** Distribution of goethite Al-substitution calculated from bulk XRD spectra according to the (U-Th)/He age of subsample. The main weathering and erosion phases in the Brownsberg area are identified in the black boxes on the right (Ero., erosion; Laterit., lateritization).

(Zachos et al., 2008; Hoorn et al., 2010; Monteiro et al., 2018; Scotese et al., 2021). It is anticipated that older duricrusts would have existed, but it was either not sampled in the present study or it was destroyed by erosion and/or subsequent weathering events. Indeed, at a global scale, compilation of lateritic and bauxitic weathering events shows a higher frequency of young ages than old ones, which probably reflects the successive processes of rejuvenation or erosion (Pidgeon et al., 2004; Shuster et al., 2005; Retallack, 2010; Monteiro et al., 2014; Riffel et al., 2015; Vasconcelos et al., 2015; Allard et al., 2018; Yans et al., 2021).

Only few dating investigations on duricrusts were made in the Guiana Shield and it is consequently particularly difficult to interpret our results in terms of local weathering events (Théveniaut and Freyssinet, 2002; Allard et al., 2018; Heller et al., 2022). Paleomagnetism dating suggests weathering episodes at 50–60 Ma (Bakhuis Mountains, Suriname; Kaw mountain, French Guiana) and ca. 10 Ma in the Guiana Shield (Moengo bauxite deposit, Suriname; Kaw mountain) (Théveniaut and Freyssinet, 2002). However, the distribution of our data suggests four major weathering episodes during the Cenozoic (**Figure 8**): 1) a lateritization event at ~35 Ma, 2) a bauxitization episode older than 15 Ma but with no more precise constraints, 3) a lateritization event at 15–20 Ma, and 4) a bauxitization event (6–2 Ma).

1) An Amazonian weathering episode ~35 Ma has been proposed in the literature (Shuster et al., 2012; Monteiro et al., 2014; Heller et al., 2022), traducing a regional weathering event in South America. However, in Suriname, the late Eocene–Oligocene is known to be the period of bauxite formation during the so called "bauxite hiatus" and must consist of particularly wet climate with a weak seasonal contrast, lower temperatures (still in the range of temperatures for tropical climates), and low sea level, increasing continental incision and drainage (Wong, 1986; Théveniaut and Freyssinet, 2002; Zachos et al., 2008). Probably, the formation of lateritic crust and bauxitic cap are

concomitant and, aside from climate, depends on environmental factors such as topography or drainage efficiency.

2) In the present study, the bauxitization in Brownsberg is not well constrained as only the goethitic coating could be dated at a maximum age of 15.5 ± 2.3 Ma (**Figure 7I**). However, the U *vs.* (U-Th)/He age graph shows a progressive precipitation of Fe-oxide with U enrichment, revealing a long-term crystallization of goethite in the bauxite sample starting ca. 15.5 Ma (**Figure 7J**). In Suriname, Bardossy and Aleva (1990) have associated the formation of the Brownsberg bauxite to the Eocene–Oligocene event (i.e., main aluminous bauxite level event) which is related to an intense weathering event related to a significant drop in the eustatic sea level that generated incision of continental areas (Wong, 1986). This would explain the lack of older age found in this area, due to intensification of drainage (i.e., increased weathering) and erosion. Goethite ages are relatively younger than this period but do not indicate the beginning of bauxitization as goethites are essentially found as coating on gibbsite. However, the observed texture of the bauxitic material (pisolithic) may reveal the physical disaggregation of a first bauxite generation during a more arid period and its redeposition with goethite cementation (Bardossy and Aleva, 1990). Still, subsequent worldwide episodes of bauxitization are recorded (Bardossy and Aleva, 1990; Retallack, 2010) and could also be related to this bauxite formation.
3) Ages of 15–20 Ma are associated with another weathering episode that has also been recorded in French Guiana (Théveniaut and Freyssinet, 2002; Heller et al., 2022). Duricrust from this interval generally contains goethite low in Al (**Figure 8D**) and can be related to a lateritization event. Heller et al. (2022) suspected this lateritization phase to be related to the mid-Miocene Climate Optimum (MMCO) and its seasonally contrasted climate with the onset on the monsoon system in Amazonia (Kaandorp et al., 2005), favorable to the formation of Fe-duricrust (Ambrosi and Nahon, 1986; Nahon and Tardy, 1992; Tardy and Roquin, 1998). The rise of the Andes, accompanied by a slight uplift of the Amazonian Shield and a marine regression (Hoorn et al., 2010; Monteiro et al., 2018; Sundell et al., 2019), led to increasing incision on the old craton and promoted weathering of exposed surfaces. This is also the process suspected to have shaped the landscape in the Carajás region, the southern part of the Brazilian shield (Monteiro et al., 2018).
4) The last weathering episode ca. 6–2 Ma revealed by our dataset was also found in French Guiana (Heller et al., 2022) and at a global scale (West Africa: Beauvais et al., 2008; Retallack, 2010; Brazil: Monteiro et al., 2014; Monteiro et al., 2018; India: Mathian et al., 2019). The high Al content in goethite from young duricrust can be linked to a bauxitization event. It is more probably associated with a global phenomenon such as the final closure of the Panama isthmus ca. 7–3 Ma and increasing precipitation (Haug and Tiedemann, 1998; Knowlton and Weigt, 1998; O'Dea et al., 2016). Various climatic proxy records (fossil phytoplankton, carbonates, etc.) highlighted a period of high atmospheric pCO_2 in the early Pliocene which could also have favored weathering reactions across the Earth at this time (Beerling and Royer, 2011; Goudie and Viles, 2012) and thus promoted the formation of laterites (Heller et al., 2022).

Dissolution and Recrystallization Processes: Implications for Duricrust Formation and Evolution

The Leo Falls lateritic cover shows a bauxitic cap above duricrust. This Fe-crust displays distinct fabric at a macroscopic scale but also different geochemical, mineralogical, and (U-Th)/He ages that highlight the long weathering history in the area. The oldest age found at the top of the Leo Falls formation (~460 m a.s.l.) in the massive duricrust (BWG13) is consistent with typical downward progression of the weathering front and chemical reorganization (Nahon and Millot, 1977; Lucas et al., 1989; Tardy, 1993; Monteiro et al., 2014). In addition, the Th/U ratio of dated generations is globally higher at the bottom of the duricrust unit (**Figure 7D, H**, **Supplementary Table S4**), as Th is relatively immobile compared to U which is mobilized under an oxidizing environment and can reveal successive dissolution/recrystallization processes of Fe-oxides (Riffel et al., 2016). Tardy et al. (1997) considered those massive duricrusts to be the first stage of duricrust formation with Fe-aggradation as goethite under a water-saturated environment, associated with a fluctuating water table. However, they considered that kaolinite cannot be preserved at this stage of weathering. In our study, remnant booklets of kaolinite have been found that suggest the epigenetic replacement of kaolinite by goethite (Nahon et al., 1989) (**Figures 5E,I**). This implies a rapid ferruginization of the saprolite unit with goethite cement at the groundwater–atmosphere interface (Heim et al., 2006) as suggested by U enrichment compared to Th, (**Figure 6B**), related to colloform goethite crystallization from U-rich fluids (Riffel et al., 2016). With the downward progression of the weathering front to form younger duricrust, REE are redistributed and enriched toward the lower part of the crust (**Figure 8C**), as observed for some other trace element in lateritic context, for example, Sc or Ni (Dublet et al., 2015; Chassé et al., 2019). The massive duricrust (BWG13) is thus progressively replaced at its base by younger duricrust in which kaolinite is replaced by the more stable gibbsite following weathering advancement, as shown by the decreasing SiO_2 concentration in other duricrusts (**Table 2**), while Fe precipitates both as hematite and goethite according to the (bio) geochemical conditions of the weathering system at the time of their formation (**Figure 4**; Trolard and Tardy, 1989).

The progression of the weathering front, from the top to the bottom, is also accompanied by an increase in Al-substitution in goethite of the younger duricrust (**Figure 8**), similar to the results of Heller et al. (2022) that give insight into physico-chemical conditions and weathering intensity. The progressive dissolution of kaolinite, which is no longer in equilibrium with the environment, starts to enrich weathering fluid in Al that can be incorporated in Al-goethite, Al-hematite, and gibbsite, more stable, under humid tropical climate (Fitzpatrick and Schwertmann, 1982; Tardy and Nahon, 1985; Fritsch et al., 2005). Aluminum enrichment in goethite can be associated

with successive cycles of dissolution and reprecipitation in the same way as metal enrichment found in goethite in other studies (Dublet et al., 2015; Chassé et al., 2019). Interestingly, Al-substitution in goethite coating found in the bauxite accounts for 0 ± 2.6 mol% (**Table 2**), while the bulk Al content is high, revealing Fe and Al segregation.

This is consistent with the idea of a concomitant formation of the massive crust (BWG13) and of the goethitic coating in BWG14 during the same lateritization episode. However, the bauxite itself (i.e., gibbsitic pisolithes) was not formed at the same time as the Fe-crust. Elsewhere, pisolithic bauxites have been observed in Brazil and Ivory Coast and were interpreted as dismantled material and development in the zone of groundwater fluctuation (Boulangé, 1984; Bardossy and Aleva, 1990). This implies that a first bauxite has been formed earlier, possibly during the main bauxite level (Théveniaut and Freyssinet, 2002), and was eroded and chemically reorganized depending on oxidizing/reducing conditions. The segregation of Al and Fe, that is, the inner concentration of Al and outward migration of Fe from gibbsite, reflects fluctuating chemical conditions and increasing O_2 partial pressure in a well-drained environment (Fitzpatrick and Schwertmann, 1982; Delvigne, 1998). This reinforces the idea that the massive duricrust (BWG13, ~460 m a.s.l.) and the Fe-cement formation in the bauxite (BWG14, ~465 m a.s.l.) occurred in a relatively short time period but were not the first stage of lateritic crust formation in the Brownsberg. Similar to the work of (Fritsch et al., 2005; Heller et al., 2022), we conclude that Al-poor goethite is formed at an early stage of profile development. Thus, Al-goethite reflects weathering advancement, Al being provided by the progressive dissolution of unstable kaolinite from BWG13. This weathering episode is also accompanied by uranium and vanadium enrichment, probably associated with successive Fe-oxide dissolution and reprecipitation and progressive fluid enrichment. But the Leo Falls crusts are already rich in those elements and attest to a longer weathering history in the Brownsberg that can be related to the duricrust boulders found in the valley which generally show older (U-Th)/He ages (**Figure 6**, **Supplementary Figure S1B**).

The morphology of a sample, its mineralogical and chemical composition, and the U and Th content of Fe-oxyhydroxides can be a tool to investigate weathering and erosion history.

CONCLUSION

This study reveals that a long weathering history has impacted Suriname and its high plateau during the Cenozoic. The oldest ages found in the Brownsberg area result from a weathering event at ca. 35 Ma. Even though previous geomorphological studies give a Paleocene–Eocene age to the Brownsberg regolith surface, this study did not allow us to reveal such old age. At the top of the plateau, the formation of massive duricrust and pisolithic bauxite are probably closely related in time, ca. 20–15 Ma, and may result from a common weathering event, associated with a fluctuating water table. This study suggests that older bauxite has formed in this area, but that has been eroded and recemented with Fe-oxide coatings, concomitantly with the formation of the massive duricrust found at the mountaintop. This can explain why boulders of various duricrust have been found downslope in the Mine, with older Fe-oxides. Subsequent lateritization events led to the downward chemical reorganization of the massive duricrust and to the formation of the lower duricrusts which exhibit distinct facies. This further chemical reworking is associated with enrichment of Al by the formation of Al-substituted goethites that are particularly gathered ca. 4 Ma and elemental enrichment such as REE, V, or Th and U, which traduce the successive dissolution/recrystallization processes.

The mineralogy and the geochemistry of lateritic cover and the geochronological investigations of Fe-oxides reveal the long-lasting tropical climate that persists in this area, allowing the formation of the Brownsberg lateritic duricrust and bauxite. This study also highlights an important erosion episode that shaped the Brownsberg mountain in the early Cenozoic.

DATA AVAILABILITY STATEMENT

The original contributions presented in the study are included in the article/**Supplementary Material**, further inquiries can be directed to the corresponding author.

AUTHOR CONTRIBUTIONS

CA: performed all experiments and helped write the whole manuscript. DC and CQ: discussion and helped with writing the whole manuscript. TA: sampling and discussion. JR and RC: field trip and sampling. BH: sampling, helped with data analysis, and discussion. RP-J and CG: He extraction, chemical analysis, and discussion on these data. SR, DV, and JN: synchrotron experiments, data analysis, and discussion on these data.

FUNDING

This work has been carried out in the framework of the French National Research Agency (ANR) RECA ANR-17-CE01-0012-01 project and the BRGM-TOTAL Source-to-Sink project and was financially supported by the French Ministry of Education and Research (CA PhD grant).

ACKNOWLEDGMENTS

We gratefully acknowledge Pr. Alexandra Courtin (GEOPS, Université Paris Saclay, France) for her help in petrography interpretations and the synchrotron μXRD experiment.

SUPPLEMENTARY MATERIAL

The Supplementary Material for this article can be found online at: https://www.frontiersin.org/articles/10.3389/feart.2022.888993/full#supplementary-material

REFERENCES

Albuquerque, M. F. d. S., Horbe, A. M. C., and Danišík, M. (2020). Episodic Weathering in Southwestern Amazonia Based on (U Th)/He Dating of Fe and Mn Lateritic Duricrust. *Chem. Geol.* 553, 119792. doi:10.1016/j.chemgeo.2020.119792

Aleva, G. J. J. (1979). Bauxite and Other Duricrust in Suriname: A Review. *Geol. Mijnb.* 58 (3), 16.

Allard, T., Gautheron, C., Bressan Riffel, S., Balan, E., Soares, B. F., Pinna-Jamme, R., et al. (2018). Combined Dating of Goethites and Kaolinites from Ferruginous Duricrusts. Deciphering the Late Neogene Erosion History of Central Amazonia. *Chem. Geol.* 479, 136–150. doi:10.1016/j.chemgeo.2018.01.004

Allard, T., Pereira, L., Mathian, M., Balan, E., Taitson Bueno, G., Falguères, C., et al. (2020). Dating Kaolinite from the Neogene Içá Formation and Overlying Laterites, Central Amazonia, Brazil: Constraints for a Stratigraphic Correlation. *Palaeogeogr. Palaeoclimatol. Palaeoecol.* 554, 109818. doi:10.1016/j.palaeo.2020.109818

Amatali, M. A. (1993). "Climate and Surface Water Hydrology," in *The Freshwater Ecosystems of Suriname*. Editor P. E. Ouboter (Dordrecht: Springer Netherlands), 29–51. doi:10.1007/978-94-011-2070-8_3

Ambrosi, J. P., and Nahon, D. (1986). Petrological and Geochemical Differentiation of Lateritic Iron Crust Profiles. *Chem. Geol.* 57 (3–4), 371–393. doi:10.1016/0009-2541(86)90059-8

Anand, R. R., Wells, M. A., Lintern, M. J., Schoneveld, L., Danišík, M., Salama, W., et al. (2021). The (U-Th)/He Chronology and Geochemistry of Ferruginous Nodules and Pisoliths Formed in the Paleochannel Environments at the Garden Well Gold Deposit, Yilgarn Craton of Western Australia: Implications for Landscape Evolution and Geochemical Exploration. *Minerals* 11 (7), 679. doi:10.3390/min11070679

Balan, E., Allard, T., Fritsch, E., Sélo, M., Falguères, C., Chabaux, F., et al. (2005). Formation and Evolution of Lateritic Profiles in the Middle Amazon Basin: Insights from Radiation-Induced Defects in Kaolinite. *Geochim. Cosmochim. Acta* 69 (9), 2193–2204. doi:10.1016/j.gca.2004.10.028

Balan, E., Fritsch, E., Allard, T., and Calas, G. (2007). Inheritance vs. Neoformation of Kaolinite during Lateritic Soil Formation: a Case Study in the Middle Amazon Basin. *Clays Clay Minerals* 55 (3), 253–259. doi:10.1346/CCMN.2007.0550303

Bardossy, G., and Aleva, G. J. J. (1990). *Lateritic Bauxites*. Development in Economic Geology.

Bassal, F., Roques, J., Corre, M., Brunet, F., Ketcham, R., Schwartz, S., et al. (2022). Role of Defects and Radiation Damage on He Diffusion in Magnetite: Implication for (U-Th)/He Thermochronology. Minerals 12, 590. doi:10.3390/min12050590

Beauvais, A., and Colin, F. (1993). Formation and Transformation Processes of Iron Duricrust Systems in Tropical Humid Environment. *Chem. Geol.* 106 (1–2), 77–101. doi:10.1016/0009-2541(93)90167-H

Beauvais, A., Ruffet, G., Hénocque, O., and Colin, F. (2008). Chemical and Physical Erosion Rhythms of the West African Cenozoic Morphogenesis: The ^{39}Ar-^{40}Ar Dating of Supergene K-Mn Oxides. *J. Geophys. Res.* 113 (F4), F04007. doi:10.1029/2008JF000996

Beerling, D. J., and Royer, D. L. (2011). Convergent Cenozoic CO2 History. *Nat. Geosci.* 4 (7), 418–420. doi:10.1038/ngeo1186

Bernal, J. P., Eggins, S. M., McCulloch, M. T., Grün, R., and Eggleton, R. A. (2006). Dating of Chemical Weathering Processes by *In Situ* Measurement of U-Series Disequilibria in Supergene Fe-Oxy/hydroxides Using LA-MC-ICPMS. *Chem. Geol.* 235 (1–2), 76–94. doi:10.1016/j.chemgeo.2006.06.009

Bird, M. I., and Chivas, A. R. (1988). Stable-isotope Evidence for Low-Temperature Kaolinitic Weathering and Post-formational Hydrogen-Isotope Exchange in Permian Kaolinites. *Chem. Geol. Isot. Geosci. Sect.* 72 (3), 249–265. doi:10.1016/0168-9622(88)90028-0

Bird, M. I., Longstaffe, F. J., Fyfe, W. S., and Bildgen, P. (1992). Oxygen-isotope Systematics in a Multiphase Weathering System in Haiti. *Geochim. Cosmochim. Acta* 56 (7), 2831–2838. doi:10.1016/0016-7037(92)90362-M

Bosma, W. (1983). Igneous and Metamorphic Complexes of the Guiana Shield in Suriname. *Geol. Mijnb.* 62, 241–254.

Boulangé, B. (1984). "Les formations bauxitiques latéritiques de côte-d'Ivoire," in Travaux et documents. Paris: ORSTOM, 341.

Bovolo, C. I., Wagner, T., Parkin, G., Hein-Griggs, D., Pereira, R., and Jones, R. (2018). The Guiana Shield Rainforests-Overlooked Guardians of South American Climate. *Environ. Res. Lett.* 13 (7), 074029. doi:10.1088/1748-9326/aacf60

Carignan, J., Hild, P., Mevelle, G., Morel, J., and Yeghicheyan, D. (2001). Routine Analyses of Trace Elements in Geological Samples Using Flow Injection and Low Pressure On-Line Liquid Chromatography Coupled to ICP-MS: A Study of Geochemical Reference Materials BR, DR-N, UB-N, AN-G and GH. *Geostand. Geoanalytical Res.* 25 (2–3), 187–198. doi:10.1111/j.1751-908X.2001.tb00595.x

Carmo, I. d. O., and Vasconcelos, P. M. (2006). 40Ar/39Ar Geochronology Constraints on Late Miocene Weathering Rates in Minas Gerais, Brazil. *Earth Planet. Sci. Lett.* 241 (1–2), 80–94. doi:10.1016/j.epsl.2005.09.056

Chassé, M., Griffin, W. L., O'Reilly, S. Y., and Calas, G. (2019). Australian Laterites Reveal Mechanisms Governing Scandium Dynamics in the Critical Zone. *Geochim. Cosmochim. Acta* 260, 292–310. doi:10.1016/j.gca.2019.06.036

Cornu, S., Montagne, D., and Vasconcelos, P. M. (2009). Dating Constituent Formation in Soils to Determine Rates of Soil Processes: A Review. *Geoderma* 153 (3–4), 293–303. doi:10.1016/j.geoderma.2009.08.006

Danišík, M., Evans, N. J., Ramanaidou, E. R., McDonald, B. J., Mayers, C., and McInnes, B. I. A. (2013). (U–Th)/He Chronology of the Robe River Channel Iron Deposits, Hamersley Province, Western Australia. *Chem. Geol.* 354, 150–162. doi:10.1016/j.chemgeo.2013.06.012

Daoust, C. (2016). *Caractérisation stratigraphique, structurale et géochimique du district minéralisé de Rosebel (Suriname) dans le cadre de l'évolution géodynamique du bouclier guyanais*. Université du Québec.

Delvigne, J. (1998). *Atlas of Micromorphology of Mineral Alteration and Weathering*. Canada: Mineralogical Association of Canada. The Canadian Mineralogist.

Deng, X.-D., Li, J.-W., and Vasconcelos, P. M. (2016). 40Ar/39Ar Dating of Supergene Mn-Oxides from the Zunyi Mn Deposit, Guizhou Plateau, SW China: Implications for Chemical Weathering and Paleoclimatic Evolution since the Late Miocene. *Chem. Geol.* 445, 185–198. doi:10.1016/j.chemgeo.2016.02.009

Derycke, A., Gautheron, C., Barbarand, J., Bourbon, P., Aertgeerts, G., Simon-Labric, T., et al. (2021). French Guiana Margin Evolution: From Gondwana Break-up to Atlantic Opening. *Terra Nova.* 33 (4), 415–422. doi:10.1111/ter.12526

Dublet, G., Juillot, F., Morin, G., Fritsch, E., Fandeur, D., and Brown, G. E., Jr. (2015). Goethite Aging Explains Ni Depletion in Upper Units of Ultramafic Lateritic Ores from New Caledonia. *Geochim. Cosmochim. Acta* 160, 1–15. doi:10.1016/j.gca.2015.03.015

Duff, M. C., Coughlin, J. U., and Hunter, D. B. (2002). Uranium Co-precipitation with Iron Oxide Minerals. *Geochim. Cosmochim. Acta* 66 (20), 3533–3547. doi:10.1016/S0016-7037(02)00953-5

Eeckhout, S. (1999). Lithology and Weathering of the Paleoproterozoic Rocks of Brownsberg (Suriname). *Bull. Société belge Géol.* 106, 117–126.

Farley, K. A., and Stockli, D. F. (2002). (U-Th)/He Dating of Phosphates: Apatite, Monazite, and Xenotime. *Rev. Mineral. Geochem.* 48 (1), 559–577. doi:10.2138/rmg.2002.48.15

Farley, K. A. (2002). (U-Th)/He Dating: Techniques, Calibrations, and Applications. *Rev. Mineral. Geochem.* 47 (1), 819–844. doi:10.2138/rmg.2002.47.18

Farley, K. A. (2018). Helium Diffusion Parameters of Hematite from a Single-Diffusion-Domain Crystal. *Geochim. Cosmochim. Acta* 231, 117–129. doi:10.1016/j.gca.2018.04.005

Fitzpatrick, R. W., and Schwertmann, U. (1982). Al-substituted Goethite-An Indicator of Pedogenic and Other Weathering Environments in South Africa. *Geoderma* 27 (4), 335–347. doi:10.1016/0016-7061(82)90022-2

Fritsch, E., Morin, G., Bedidi, A., Bonnin, D., Balan, E., Caquineau, S., et al. (2005). Transformation of Haematite and Al-Poor Goethite to Al-Rich Goethite and Associated Yellowing in a Ferralitic Clay Soil Profile of the Middle Amazon Basin (Manaus, Brazil). *Eur. J. Soil Sci.* 56 (5), 575–588. doi:10.1111/j.1365-2389.2005.00693.x

Gautheron, C., and Zeitler, P. K. (2020). Noble Gases Deliver Cool Dates from Hot Rocks. *Elements* 16 (5), 303–309. doi:10.2138/gselements.16.5.303

Gautheron, C., Pinna-Jamme, R., Derycke, A., Ahadi, F., Sanchez, C., Haurine, F., et al. (2021). Technical Note: Analytical Protocols and Performance for Apatite and Zircon (U–Th)/He Analysis on Quadrupole and Magnetic Sector Mass Spectrometer Systems between 2007 and 2020. *Geochronology* 3 (1), 351–370. doi:10.5194/gchron-3-351-2021

Girard, J.-P., Freyssinet, P., and Chazot, G. (2000). Unraveling Climatic Changes from Intraprofile Variation in Oxygen and Hydrogen Isotopic Composition of Goethite and Kaolinite in Laterites: An Integrated Study from Yaou, French Guiana. *Geochim. Cosmochim. Acta* 64 (3), 409–426. doi:10.1016/S0016-7037(99)00299-9

Goudie, A. S., and Viles, H. A. (2012). Weathering and the Global Carbon Cycle: Geomorphological Perspectives. *Earth Sci. Rev.* 113 (1–2), 59–71. doi:10.1016/j.earscirev.2012.03.005

Guinoiseau, D., Fekiacova, Z., Allard, T., Druhan, J. L., Balan, E., and Bouchez, J. (2021). Tropical Weathering History Recorded in the Silicon Isotopes of Lateritic Weathering Profiles. *Geophys. Res. Lett.* 48 (19), e2021GL092957. doi:10.1029/2021GL092957

Haug, G. H., and Tiedemann, R. (1998). Effect of the Formation of the Isthmus of Panama on Atlantic Ocean Thermohaline Circulation. *Nature* 393 (6686), 673–676. doi:10.1038/31447

Hénocque, O., Ruffet, G., Colin, F., and Féraud, G. (1998). 40Ar/39Ar Dating of West African Lateritic Cryptomelanes. *Geochim. Cosmochim. Acta* 62 (16), 2739–2756. doi:10.1016/S0016-7037(98)00185-9

Heim, J. A., Vasconcelos, P. M., Shuster, D. L., Farley, K. A., and Broadbent, G. (2006). Dating Paleochannel Iron Ore by (U-Th)/He Analysis of Supergene Goethite, Hamersley Province, Australia. *Geology* 34 (3), 173. doi:10.1130/G22003.1

Heller, B. M., Riffel, S. B., Allard, T., Morin, G., Roig, J.-Y., Couëffé, R., et al. (2022). Reading the Climate Signals Hidden in Bauxite. *Geochim. Cosmochim. Acta* 323, 40–73. doi:10.1016/j.gca.2022.02.017

Hofmann, F., Reichenbacher, B., and Farley, K. A. (2017). Evidence for >5 Ma Paleo-Exposure of an Eocene-Miocene Paleosol of the Bohnerz Formation, Switzerland. *Earth Planet. Sci. Lett.* 465, 168–175. doi:10.1016/j.epsl.2017.02.042

Hofmann, F., Treffkorn, J., and Farley, K. A. (2020). U-loss Associated with Laser-Heating of Hematite and Goethite in Vacuum during (U-Th)/He Dating and Prevention Using High O2 Partial Pressure. *Chem. Geol.* 532, 119350. doi:10.1016/j.chemgeo.2019.119350

Hoorn, C., Wesselingh, F. P., ter Steege, H., Bermudez, M. A., Mora, A., Sevink, J., et al. (2010). Amazonia through Time: Andean Uplift, Climate Change, Landscape Evolution, and Biodiversity. *Science* 330 (6006), 927–931. doi:10.1126/science.1194585

Jeffery, M. L., Poulsen, C. J., and Ehlers, T. A. (2012). Impacts of Cenozoic Global Cooling, Surface Uplift, and an Inland Seaway on South American Paleoclimate and Precipitation 18O. *Geol. Soc. Am. Bull.* 124 (3–4), 335–351. doi:10.1130/B30480.1

Kaandorp, R. J. G., Vonhof, H. B., Wesselingh, F. P., Pittman, L. R., Kroon, D., and van Hinte, J. E. (2005). Seasonal Amazonian Rainfall Variation in the Miocene Climate Optimum. *Palaeogeogr. Palaeoclimatol. Palaeoecol.* 221 (1–2), 1–6. doi:10.1016/j.palaeo.2004.12.024

Kerisit, S., Felmy, A. R., and Ilton, E. S. (2011). Atomistic Simulations of Uranium Incorporation into Iron (Hydr)Oxides. *Environ. Sci. Technol.* 45 (7), 2770–2776. doi:10.1021/es1037639

King, L. C. (1962). *The Morphology of the Earth : A Study and Synthesis of World Scenery (1 Vol)*. Edinburgh: Oliver & Boyd.

Knowlton, N., and Weigt, L. A. (1998). New Dates and New Rates for Divergence across the Isthmus of Panama. *Proc. R. Soc. Lond. Ser. B Biol. Sci.* 265 (1412), 2257–2263. doi:10.1098/rspb.1998.0568

Kroonenberg, S. B., de Roever, E. W. F., Fraga, L. M., Reis, N. J., Faraco, T., Lafon, J.-M., et al. (2016). Paleoproterozoic Evolution of the Guiana Shield in Suriname: A Revised Model. *Neth. J. Geosci.* 95 (04), 491–522. doi:10.1017/njg.2016.10

Leclercq, N., Berthault, J., Langlois, F., Le, S., and Poirier, S. (2015). "FLYSCAN: a Fast and Multi-Technique Data Acquisition Platform for the SOLEIL Beamlines," in International Conference on Accelerator & Large Experimental Physics Control Systems (Melbourne, Australia: ICALPECS), 826–829.

Levett, A., Gagen, E. J., Diao, H., Guagliardo, P., Rintoul, L., Paz, A., et al. (2019). The Role of Aluminium in the Preservation of Microbial Biosignatures. *Geosci. Front.* 10 (3), 1125–1138. doi:10.1016/j.gsf.2018.06.006

Lucas, Y., Kobilsek, B., and Chauvel, A. (1989). Structure, Genesis, and Present Evolution of Amazonian Bauxites Developed on Sediments. *Trav. ICSOBA* 19, 81–94.

Lucas, Y., Luizao, F. J., Chauvel, A., Rouiller, J., and Nahon, D. (1993). The Relation between Biological Activity of the Rain Forest and Mineral Composition of Soils. *Science* 260 (5107), 521–523. doi:10.1126/science.260.5107.521

Mathian, M., Aufort, J., Braun, J.-J., Riotte, J., Selo, M., Balan, E., et al. (2019). Unraveling Weathering Episodes in Tertiary Regoliths by Kaolinite Dating (Western Ghats, India). *Gondwana Res.* 69, 89–105. doi:10.1016/j.gr.2018.12.003

Mathian, M., Bueno, G. T., Balan, E., Fritsch, E., Do Nascimento, N. R., Selo, M., et al. (2020). Kaolinite Dating from Acrisol and Ferralsol: A New Key to Understanding the Landscape Evolution in NW Amazonia (Brazil). *Geoderma* 370, 114354. doi:10.1016/j.geoderma.2020.114354

Missana, T., Garcı´a-Gutiérrez, M., and Maffiotte, C. (2003). Experimental and Modeling Study of the Uranium (VI) Sorption on Goethite. *J. Colloid Interface Sci.* 260 (2), 291–301. doi:10.1016/S0021-9797(02)00246-1

Monsels, D. A. (2016). Bauxite Deposits in Suriname: Geological Context and Resource Development. *Neth. J. Geosci. Geol.* 95 (4), 405–418. doi:10.1017/njg.2015.28

Monteiro, H. S., Vasconcelos, P. M., Farley, K. A., Spier, C. A., and Mello, C. L. (2014). (U-Th)/He Geochronology of Goethite and the Origin and Evolution of Cangas. *Geochim. Cosmochim. Acta* 131, 267–289. doi:10.1016/j.gca.2014.01.036

Monteiro, H. S., Vasconcelos, P. M. P., Farley, K. A., and Lopes, C. A. M. (2018). Age and Evolution of Diachronous Erosion Surfaces in the Amazon: Combining (U-Th)/He and Cosmogenic 3He Records. *Geochim. Cosmochim. Acta* 229, 162–183. doi:10.1016/j.gca.2018.02.045

Nahon, D., and Millot, G. (1977). V. Enfoncement géochimique des cuirasses ferrugineuses par épigénie du manteau d'altération des roches mères gréseuses. Influence sur le paysage. *Sci. Géologiques. Bull.* 30 (4), 275–282. doi:10.3406/sgeol.1977.1523

Nahon, D., and Tardy, Y. (1992). "The Ferruginous Laterites," in Handbook of Exploration Geochemistry. Amsterdan, Netherlands: Elsevier Science, 41–55. doi:10.1016/B978-0-444-89095-5.50010-9

Nahon, D. B., Herbillon, A. J., and Beauvais, A. (1989). The Epigenetic Replacement of Kaolinite by Lithiophorite in a Manganese-Lateritic Profile, Brazil. *Geoderma* 44 (4), 247–259. doi:10.1016/0016-7061(89)90034-7

Nahon, D. B. (1991). Self-organization in Chemical Lateritic Weathering. *Geoderma* 51 (1–4), 5–13. doi:10.1016/0016-7061(91)90063-Y

O'Dea, A., Lessios, H. A., Coates, A. G., Eytan, R. I., Restrepo-Moreno, S. A., Cione, A. L., et al. (2016). Formation of the Isthmus of Panama. *Sci. Adv.* 2 (8), e1600883. doi:10.1126/sciadv.1600883

Pidgeon, R. T., Brander, T., and Lippolt, H. J. (2004). Late Miocene (U+Th)-4He Ages of Ferruginous Nodules from Lateritic Duricrust, Darling Range, Western Australia. *Aust. J. Earth Sci.* 51 (6), 901–909. doi:10.1111/j.1400-0952.2004.01094.x

Ravel, B., and Newville, M. (2005). ATHENA, ARTEMIS, HEPHAESTUS : Data Analysis for X-Ray Absorption Spectroscopy Using IFEFFIT. *J. Synchrotron Radiat.* 12 (4), 537–541. doi:10.1107/S0909049505012719

Retallack, G. J. (2010). Lateritization and Bauxitization Events. *Econ. Geol.* 105 (3), 655–667. doi:10.2113/gsecongeo.105.3.655

Riffel, S. B., Vasconcelos, P. M., Carmo, I. O., and Farley, K. A. (2015). Combined 40Ar/39Ar and (U-Th)/He Geochronological Constraints on Long-Term Landscape Evolution of the Second Paraná Plateau and its Ruiniform Surface Features, Paraná, Brazil. *Geomorphology* 233, 52–63. doi:10.1016/j.geomorph.2014.10.041

Riffel, S. B., Vasconcelos, P. M., Carmo, I. O., and Farley, K. A. (2016). Goethite (U-Th)/He Geochronology and Precipitation Mechanisms during Weathering of Basalts. *Chem. Geol.* 446, 18–32. doi:10.1016/j.chemgeo.2016.03.033

Rudnick, R. L., and Gao, S. (2003). Composition of the Continental Crust. *Treatise Geochem.* 3, 1–64. doi:10.1016/b0-08-043751-6/03016-4

Ruffet, G., Innocent, C., Michard, A., Féraud, D., Beauvais, A., Nahon, D., et al. (1996). A Geochronological 40Ar/39Ar and 87Rb/87Sr Study of K-Mn Oxides from the Weathering Sequence of Azul, Brazil. *Geochim. Cosmochim. Acta* 60 (12), 2219–2232. doi:10.1016/0016-7037(96)00080-4

Schulze, D. G. (1984). The Influence of Aluminium on Iron Oxides. VIII. Unit-Cell Dimensions of Al-Substituted Goethites and Estimation of Al from Them. *Clays Clay Minerals* 32 (1), 36–44. doi:10.1346/ccmn.1984.0320105

Schwertmann, U., and Carlson, L. (1994). Aluminum Influence on Iron Oxides: XVII. Unit-Cell Parameters and Aluminum Substitution of Natural Goethites. *Soil Sci. Soc. Am. J.* 58 (1), 256–261. doi:10.2136/sssaj1994.03615995005800010039x

Scotese, C. R., Song, H., Mills, B. J. W., and van der Meer, D. G. (2021). Phanerozoic Paleotemperatures: The Earth's Changing Climate during the Last 540 Million Years. *Earth-Science Rev.* 215, 103503. doi:10.1016/j.earscirev.2021.103503

Shuster, D. L., Vasconcelos, P. M., Heim, J. A., and Farley, K. A. (2005). Weathering Geochronology by (U-Th)/He Dating of Goethite. *Geochim. Cosmochim. Acta* 69 (3), 659–673. doi:10.1016/j.gca.2004.07.028

Shuster, D. L., Farley, K. A., Vasconcelos, P. M., Balco, G., Monteiro, H. S., Waltenberg, K., et al. (2012). Cosmogenic 3He in Hematite and Goethite from Brazilian "Canga" Duricrust Demonstrates the Extreme Stability of These Surfaces. *Earth Planet. Sci. Lett.* 329–330, 41–50. doi:10.1016/j.epsl.2012.02.017

Solé, V. A., Papillon, E., Cotte, M., Walter, Ph., and Susini, J. (2007). A Multiplatform Code for the Analysis of Energy-Dispersive X-Ray Fluorescence Spectra. *Spectrochim. Acta Part B At. Spectrosc.* 62 (1), 63–68. doi:10.1016/j.sab.2006.12.002

Spear, F. S., and Pyle, J. M. (2002). Apatite, Monazite, and Xenotime in Metamorphic Rocks. *Rev. Mineral. Geochem.* 48 (1), 293–335. doi:10.2138/rmg.2002.48.7

Stallard, R. F. (1988). "Weathering and Erosion in the Humid Tropics," in *Physical and Chemical Weathering in Geochemical Cycles*. Editors A. Lerman and M. Meybeck (Dordrecht: Springer Netherlands), 225–246. doi:10.1007/978-94-009-3071-1_11

Sundell, K. E., Saylor, J. E., Lapen, T. J., and Horton, B. K. (2019). Implications of Variable Late Cenozoic Surface Uplift across the Peruvian Central Andes. *Sci. Rep.* 9 (1), 4877. doi:10.1038/s41598-019-41257-3

Tardy, Y., and Nahon, D. (1985). Geochemistry of Laterites, Stability of Al-Goethite, Al-Hématite, and Fe3+-Kaolinite in Bauxites and Ferricretes: An Approach to the Mechanism of Concretion Formation. *Am. J. Sci.* 285, 865–903. doi:10.2475/ajs.285.10.865

Tardy, Y., and Roquin, C. (1998). *Dérive des continents, Paléoclimats et altérations tropicales (1 vol)*. Orléans, France: BRGM.

Tardy, Y., Boeglin, J.-L., and Roquin, C. (1997). *Petrological and Geochemical Classification of Bauxites and Their Associated Iron-Rich Laterites*. USP, São Paulo; OSTOM, Paris: Brazilian Bauxites, 23–49.

Tardy, Y. (1993). *Pétrologie des latérites et des sols tropicaux*. Paris, France: Masson.

Taylor, S. R., and McLennan, S. M. (1995). The Geochemical Evolution of the Continental Crust. *Rev. Geophys.* 33 (2), 241–265. doi:10.1029/95rg00262

Théveniaut, H., and Freyssinet, Ph. (1999). Paleomagnetism Applied to Lateritic Profiles to Assess Saprolite and Duricrust Formation Processes: the Example of Mont Baduel Profile (French Guiana). *Palaeogeogr. Palaeoclimatol. Palaeoecol.* 148 (4), 209–231. doi:10.1016/S0031-0182(98)00183-7

Théveniaut, H., and Freyssinet, P. (2002). Timing of Lateritization on the Guiana Shield: Synthesis of Paleomagnetic Results from French Guiana and Suriname. *Palaeogeogr. Palaeoclimatol. Palaeoecol.* 178 (1–2), 91–117. doi:10.1016/S0031-0182(01)00404-7

Trolard, F., and Tardy, Y. (1989). A Model of Fe3+-Kaolinite, Al3+-Goethite, Al3+-Hematite Equilibria in Laterites. *Clay Miner.* 24, 1–21. doi:10.1180/claymin.1989.024.1.01

van der Hammen, T., and Hooghiemstra, H. (2000). Neogene and Quaternary History of Vegetation, Climate, and Plant Diversity in Amazonia. *Quat. Sci. Rev.* 19, 725–742. doi:10.1016/S0277-3791(99)00024-4

van der Hammen, T., and Wymstra, T. A. (1964). A Palynological Study on the Tertiary and Upper Cretaceous of British Guiana. *Leisde Geol. Meded.* 30 (1), 183–241.

Vantelon, D., Trcera, N., Roy, D., Moreno, T., Mailly, D., Guilet, S., et al. (2016). The LUCIA Beamline at SOLEIL. *J. Synchrotron Radiat.* 23 (2), 635–640. doi:10.1107/S1600577516000746

Vasconcelos, M., Renne, P. R., Brimhall, G. H., and Becker, T. A. (1994). Direct Dating of Weathering Phenomena by 40Ar/39Ar and K-Ar Analysis of Supergene K-Mn Oxides. *Geochim. Cosmochim. Acta* 58 (6), 31. doi:10.1016/0016-7037(94)90565-7

Vasconcelos, P. M., Heim, J. A., Farley, K. A., Monteiro, H., and Waltenberg, K. (2013). 40Ar/39Ar and (U-Th)/He-4He/3He Geochronology of Landscape Evolution and Channel Iron Deposit Genesis at Lynn Peak, Western Australia. *Geochim. Cosmochim. Acta* 117, 283–312. doi:10.1016/j.gca.2013.03.037

Vasconcelos, P. M., Reich, M., and Shuster, D. L. (2015). The Paleoclimatic Signatures of Supergene Metal Deposits. *Elements* 11 (5), 317–322. doi:10.2113/gselements.11.5.317

Vermeesch, P., Seward, D., Latkoczy, C., Wipf, M., Günther, D., and Baur, H. (2007). α-Emitting Mineral Inclusions in Apatite, Their Effect on (U-Th)/He Ages, and How to Reduce it. *Geochim. Cosmochim. Acta* 71 (7), 1737–1746. doi:10.1016/j.gca.2006.09.020

Wells, M. A., Danišík, M., McInnes, B. I. A., and Morris, P. A. (2019). (U-Th)/He-dating of Ferruginous Duricrust: Insight into Laterite Formation at Boddington, WA. *Chem. Geol.* 522, 148–161. doi:10.1016/j.chemgeo.2019.05.030

Westerhold, T., Marwan, N, Drury, A. J., Liebrand, D., Agnini, C., Anagnostou, E., et al. (2020). An Astronomically Dated Record of Earth's Climate and its Predictability over the Last 66 Million Years. *Science* 369 (6509), 1383–1387. doi:10.1126/science.aba6853

Wong, T. E. (1986). Outline of the Stratigraphy and the Geological History of the Suriname Coastal Plain. *Geol. Mijnb.* 65, 223–241.

Wong, T. E. (1994). The Paleocene-Eocene Succession in the Guiana Basin. *Bull. Société belge Géologie* 103 (3–4), 281–291.

Yans, J., Verhaert, M., Gautheron, C., Antoine, P.-O., Moussi, B., Dekoninck, A., et al. (2021). (U-Th)/He Dating of Supergene Iron (Oxyhydr-)Oxides of the Nefza-Sejnane District (Tunisia): New Insights into Mineralization and Mammalian Biostratigraphy. *Minerals* 11 (3), 260. doi:10.3390/min11030260

Yapp, C. J., and Shuster, D. L. (2011). Environmental Memory and a Possible Seasonal Bias in the Stable Isotope Composition of (U-Th)/He-Dated Goethite from the Canadian Arctic. *Geochim. Cosmochim. Acta* 75 (15), 4194–4215. doi:10.1016/j.gca.2011.04.029

Yapp, C. J., and Shuster, D. L. (2017). D/H of Late Miocene Meteoric Waters in Western Australia: Paleoenvironmental Conditions Inferred from the δD of (U-Th)/He-Dated CID Goethite. *Geochim. Cosmochim. Acta* 213, 110–136. doi:10.1016/j.gca.2017.06.036

Zachos, J. C., Dickens, G. R., and Zeebe, R. E. (2008). An Early Cenozoic Perspective on Greenhouse Warming and Carbon-Cycle Dynamics. *Nature* 451 (7176), 279–283. doi:10.1038/nature06588

Conflict of Interest: The authors declare that the research was conducted in the absence of any commercial or financial relationships that could be construed as a potential conflict of interest.

Publisher's Note: All claims expressed in this article are solely those of the authors and do not necessarily represent those of their affiliated organizations or those of the publisher, the editors, and the reviewers. Any product that may be evaluated in this article, or claim that may be made by its manufacturer, is not guaranteed or endorsed by the publisher.